POLARIZATION INDEPENDENT SPECTRAL PHASE COMPENSATION AND SHAPING OF FEMTOSECOND OPTICAL PULSES USING QUARTER WAVE-PLATE AND SINGLE-LAYER LIQUID CRYSTAL MODULATOR

A Thesis

Submitted to the Faculty

of

Purdue University

by

Catherine Gail Slater

In Partial Fulfillment of the

Requirements for the Degree

of

Master of Science in Electrical and Computer Engineering

May 2005

This thesis is dedicated to my sister, Mary, for always being there when I was stressed and needed a helping hand or someone to keep an eye on me, and to my parents for their continuous support and encouragement.

ACKNOWLEDGMENTS

First and foremost, I would like to thank Professor A.M. Weiner for providing the opportunity to perform research towards this thesis and for guiding me along the way. His vision and focus with this thesis idea has been been incredible. Thanks also to Dr. Dan Leaird for consistently answering questions while I was in the lab and for helping me stay on track even when faced with a multitude of hurdles throughout the duration of this research. In addition, I would like to thank Dr. Bill Oakes for encouraging me to pursue teaching and Dr. Ragu Balakrishnan for stimulating me through his enthusiasm towards graduate school and also for allowing me to learn under him in my most recent teaching endeavors. Thanks also goes to Al and Nate for helping me out when I did not understand theory in my various endeavors and for providing much needed amounts of encouragement when I was having trouble. I would also like to thank Ryan for answering some questions regarding his previous experiments. My gratitude is also expressed to Professors Mark R. Bell and William J. Chappell for participating in the final overview of this project. Finally, I am grateful for the opportunity to study at Purdue, where the atmosphere is very conducive to pursuing educational advancement through research.

TABLE OF CONTENTS

Page

Page

LIST OF TABLES

LIST OF FIGURES

SYMBOLS

Roman

a		semi-major axis of an ellipse
b		semi-minor axis of an ellipse
B		magnetic field
c		velocity of light in a vacuum (about 3×10^8m/s)
d		spacing between grooves on a grating
D		detector
	or	electric field intensity
E		electric field or e-field
f		focal length of a lens
H		magnetic field intensity
j		imaginary number of value $\sqrt{-1}$
k		propagation constant $\frac{\omega n}{c}$
K		time-bandwidth product
L		distance between LCM layer and reflective mirror
m		diffraction order
n		index of diffraction (dimensionless)
V		voltage
w		Gaussian beam radius or width or spot size

Greek

α		azimuth of an ellipse
	or	angle of incidence for a grating
	or	amount of SMF that can be compensated by 1m DCF

β		angle of diffraction for a grating
γ		angle variable in a Jones vector specifying polarization axis
ϵ		time-varying real-valued field
η_e		extraordinary ray refraction index
η_o		ordinary ray refraction index
θ		angle of rotation for a polarizer
	or	facet angle of a grating
λ		wavelength
π		irrational ratio of the circumference of a circle to its diameter
ζ		phase difference betwen axes of a waveplate
τ		time delay
ϕ		phase of a field
	or	rotation matrix angle
Ψ		phase difference between fields abbreviated phase angle
ν		frequency of signal
ω		angular frequency expressed in rad/s

Math

$\approx$	approximately equal to
$\triangleq$	by definition, defined as
$\wedge$	"carrot" denotes a unit magnitude direction vector
$\triangle$	change in
bold	denotes a vector quantity
subscript	denotes appended information
∂	partial derivative
$\times$	vector cross product

ABBREVIATIONS

CW	Continuous Wave
DCF	Dispersion Compensating Fiber
FBG	Fiber Bragg Grating
FWHM	Full Width at Half Maximum
HWP	Half Wave Plate
IR	InfraRed
ISI	Intersymbol Interference
ITO	Indium Tin Oxide
LC	Liquid Crystal
LCM	Liquid Crystal Modulator
LHCP	Left-Handed Circular Polarization
OSA	Optical Spectrum Analyzer
PDL	Polarization Dependent Loss
QW	Quarter Wave
QWP	Quarter Wave Plate
RMS	Root Mean Square
SLM	Spatial Light Modulator
SMF	Single-Mode Fiber
SOP	State Of Polarization
TDM	Time Division Multiplexing
WDM	Wavelength Division Multiplexing

GLOSSARY

aberration	Deviation from the norm.
achromatic lens	Lens that is corrected to bring two specified wavelengths to a common focal point. Constructed of two lenses that together minimize the signal distortion.
additive pulse	Process of shortening pulse width by using nonlinear effects in an external cavity to produce a phase-distorted pulse that can be added to the pulse in the main cavity to cancel the wings.
amplitude	Maximum value of the electromagnetic wave.
anamorphic magnification	Directions of maximum and minimum magnification are orthagonal.
angular frequency	Oscillation measured in radians/second.
bandwidth	Range of frequencies over which the component is designed to function.
bandwidth-limited	Limitation of the system performance caused by bandwidth (as opposed to the amplitude of the signal)

beam waist	Point in a Gaussian beam in which the minimum beam diameter occurs.
birefringence	Separation of optical signal when incident on a doubly refracting object into two diverging beams. The diverging beams are called the ordinary and extraordinary beams.
bit	Binary digit. Either 0 or 1. Represents the information in a digital system.
bit rate	Speed at which the information is modulated within the system.
C-band	Optical frequencies from 1530 nm to 1565 nm.
channel	Medium over which the information travels in communication.
chirped	Rapid changing or 'ringing' of the pulse.
chromatic dispersion	Dispersion of the pulse due to the different speeds at which different wavelength components travel in a fiber.
closed-loop	A system that compensates itself by using a learned electronics control.
collimate	Process in which a beam is converted into a parallel beam as opposed to a divergent beam.

communications	Process of tranmitting data from a transmitter to a receiver.
dBm	Unit of power in which Decibels are referenced to one milliwatt.
dispersion	Separation of a beam into its many wavelength components.
dispersion compensating fiber (DCF)	Fiber used to compensate the dispersion caused by single mode fiber. It has an opposite refractive index from single mode fiber.
erbium	Ions commonly added to a material to create lasing.
extraordinary axis	Axis along which the extraordinary ray lies.
extraordinary ray	Ray that does not necessarily follow Snell's law of refraction in a doubly refracting crystal. See also: birefrengence.
fiber Bragg gratings	A grating that can reflect a predetermined range of wavelengths of light while passing all other wavelengths of light by taking advantage of the effective reflection coefficient of an optical waveguide.

fiber ring laser	Laser that uses fiber to produce a standing wave pattern and stimulated emission through resonance in the fiber. The ring can have single directional or bi-directional transmission of the light in practical applications.
focal length	Distance from the lens to the point at which the beam is focused.
focal plane	Plane that includes the focal point and is perpendicular to the direction of propagation of the optical signal.
free-space	Air.
frequency	Number of wavelengths that pass a fixed point in a given time.
full-width at half maximum (FWHM)	Difference between the two time values at which the signal amplitude is half of the maximum.
grating	Optical device that has an arrangement of 'lines' that is used to disperse light.
grating spacing	Grating ability to separate wavelengths equal to the number of lines per millimeter.

group	Group of waves that have slightly different individual frequencies. Envelope determined by the additive resultant of the group of waves as it travels through a component.
group velocity	Velocity of the group with respect to angular frequency.
intersymbol interference	Interferece in a stream of modulated bits that results from pulse dispersion and overlapping of pulse edges. Can lead to decoding errors at the receiver.
L-band	Optical frequencies from 1565 nm to 1625 nm.
liquid crystal modulator (LCM)	See spatial light modulator.
mode-locked	Process of locking the phases of the laser modes to produce an ultrashort pulse.
modulation	Series of contrast in the lines and spaces from the images of a lens.
open-loop	System that operates without feedback.
optical communications	Transmission and reception of messages and information through use of optical devices.
optical spectral analyzer (OSA)	Device used to analyze the electromagnetic spectrum of an optical signal.

phase difference	Effective difference in the phase of the extraordinary and ordinary rays in a birefrengent material.
polarization	Direction of the electric field vector with respect to the direction of propagation of the wave.
resolution	Minimum adjustment able to be achieved on LCM.
single mode fiber (SMF)	Optical waveguide in which only the lowest order mode is bound that allows a pair of orthagonally polarized fields to propagate.
spatial light modulator (SLM)	Component used for optical data processing. It implies a phase to the signal by causing a change in the electromagnetic field through control of dipoles induced in liquid crystal.
spectral phase	Particular point in the spectrum measured from an arbitrary zero and expressed in terms of an angle.
spectral range	Spectral width. Wavelength interval over which the magnitude of the signal is greater than one half of the maximum. Specified in terms of FWHM.
spectrum	Ordered array of the wave components.
temporal	Related to time.

temporal window effect	Time domain limitation of data transmission and reception resulting from the active area size with respect to the beam.
temporally broadened	Spread in time.
time division multiplexing (TDM)	Process of sending more than one signal over a single channel by using different time intervals for different signals.
transverse wave	A specific wave in which the fields lie orthagonal to the direction of wave propagation.
tunability	Precision.
wavelength division multiplexing (WDM)	Process of sending more than one signal over a single channel by assigning each signal a different frequency band at which it propagates.

ABSTRACT

Slater, Catherine Gail. M.S.E.C.E, Purdue University, May, 2005. Polarization Independent Spectral Phase Compensation and Shaping of Femtosecond Optical Pulses Using Quarter Wave-Plate and Single-Layer Liquid Crystal Modulator. Major Professor: Andrew M. Weiner.

Previously, a polarization independent chromatic dispersion compensator to restore a temporally broadened optical pulse to its original width after transmitting through a dispersive system was developed with polarization insensitivity, fine-tunability and low loss. This is of particular importance because chromatic dispersion in optical fiber is a fundamental limiting barrier on the bit rate-distance product in optical communication systems. The previous system was based on a liquid crystal modulator array and diffraction grating technology, and was demonstrated to be applicable in both wavelength-division multiplexing (WDM) and time-division multiplexing (TDM) optical communications. The previous system utilized reflection geometry to minimize power loss. It had an extremely low polarization-dependent loss and could thus work with an arbitrary input state of polarization. One difficultly with this apparatus was the rather complex two-layer modulator technology required in order to achieve polarization independence. Addressing this deficiency by modifying the pulse shaping apparatus to utilize a single layer modulator array is the focus of the research described by this thesis. After repeating the experiments, the two-layer device was replaced with a single-layer LCM and a quarter wave-plate; a design that is much more economical than the previous setup. The experiments were once again repeated to demonstrate the polarization insensitivity and fine-tunability.

1. INTRODUCTION

1.1 Narrative of Problem

Optical communication is the process of transmitting messages between a sender and a recipient through use of optical fiber to transmit the information. The data is modulated onto the fiber as quickly as possible because a message with any significant meaning contains millions of bits. The bit rate is limited by dispersion, which causes short pulses to temporally broaden as they propagate in the fiber. As a result, the binary coding cannot be modulated any faster than the dispersed width of the signal or intersymbol interference (ISI) will occur. If the binary coding is modulated faster than this speed, the distance at which the information is useful is shortened significantly, as illustrated by figure 1.1 [1]. The capacity limitations of the fiber link are described by the product of the bit rate and the transmission length or distance, called the bit rate-distance product.

Single-mode fiber (SMF) dispersion is mainly caused by the broadening of wavelength components of the pulse traveling at slightly different velocities within the fiber. This phenomena is referred to as chromatic dispersion and is illustrated graphically in figure 1.2 [2].

1.2 Prior Knowledge

Dispersion compensating fibers (DCFs) and chirped fiber Bragg gratings (FBGs) are currently used to compensate for the chromatic dispersion to restore a temporally broadened pulse to its original width [2, 3].

Each of the chromatic dispersion compensation methods has advantages and disadvantages. Chirped FBGs are limited to their ability to be tuned for compensation

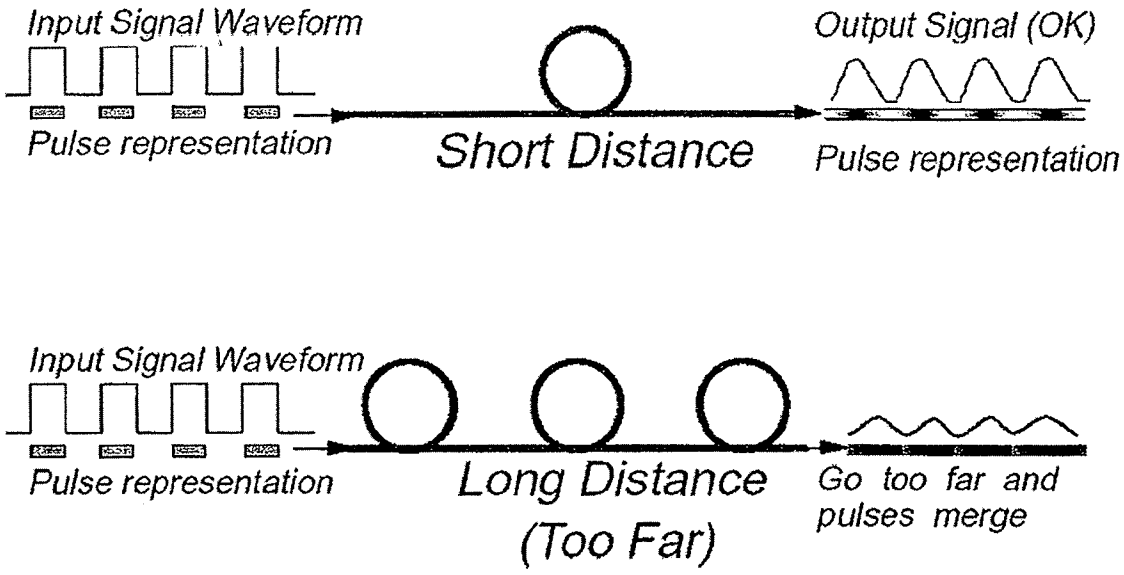

Fig. 1.1. The distance at which the information is useful is dependent on the speed of data modulation. If modulation is faster than the dispersed width of the signal, ISI occurs and proper decoding cannot be guaranteed at the receiver. Effects of dispersion are evident by (A) shorter length of fiber causing a small amount of disturbance in the signal reception and (B) longer length of fiber causing a significant distortion of the signal.

and can only handle one wavelength division multiplexing (WDM) channel at a time. DCF compensation results in pulses with higher order dispersion and also does not have fine-tunability capabilities. Both, however, restore the pulse to its original state as a bandwidth-limited pulse, as illustrated in figure 1.3.

Spatial light modulators (SLMs) have also been used to compensate the chromatic dispersion of a temporally broadened pulse. A previous system was based on a liquid crystal modulator (LCM) array and diffraction grating technology [4]. The system was demonstrated to be applicable in both wavelength-division multiplexing (WDM) and time-division multiplexing (TDM) optical communications. It utilized a Fourier Transform pulse shaper and reflection geometry to minimize power loss. Finally, it could work with an arbitrary input state of polarization due to the extremely

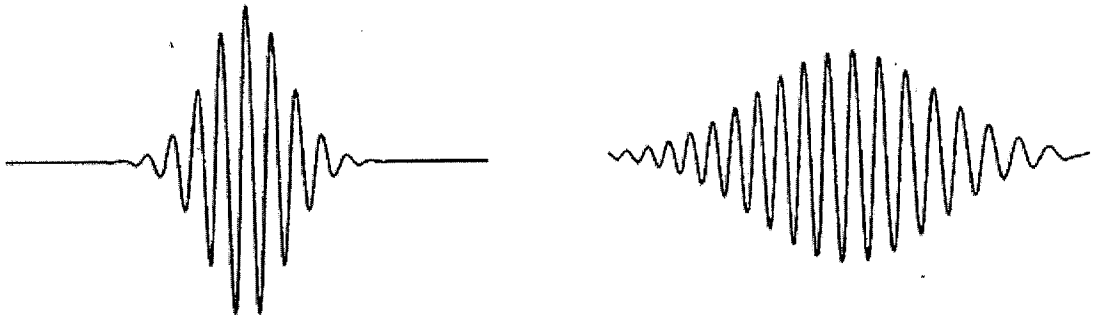

Fig. 1.2. Chromatic dispersion of a chirped Gaussian Pulse [2].

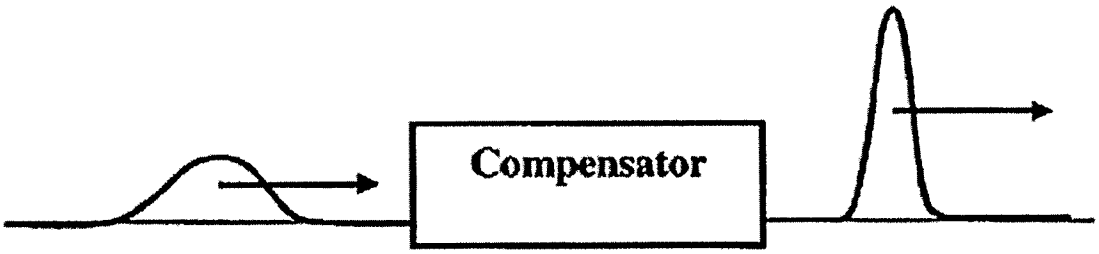

Fig. 1.3. Effects of dispersion are reduced by a compensator, which functions to retore a temporally broadened optical pulse to the original nearly bandwidth-limited pulse.

low polarization-dependent loss. The setback to this method is the rather complex two-layer modulator technology required to achieve polarization independence.

1.3 New Knowledge

The forthcoming thesis demonstrates a method to overcome the complexities related to using the two-layer SLM modulator technology while still maintaining polarization insensitivity. This difficiency was addressed by modifying the pulse shaping apparatus to utilize a single layer modulator array by replacing the two-layer device with a single-layer LCM and a quarter wave-plate. The new design is

much more economical than the previous setup, while still maintaining polarization independent phase compensation with low loss. It has been demonstrated, as with the aforementioned system, to have an extremely low polarization-dependent loss and the ability to work with an aribtrary and time-varying state of polarization (SOP).

1.4 Preview of Other Chapters

After revealing the background information and mathematics required to understand the theory behind dispersion, dispersion compensation, pulse shaping, polarization independence, and the differences between the two-layer and single-layer liquid crystal technologies, each of these topics will be discussed in detail. Two types of dispersion compensating fiber (DCF) were investigated and will be discussed immediately following the mathematics. Next, the intricacies of pulse shaping will be discussed, followed by the details specific to polarization independent pulse shaping, as applied to each of the two systems. Finally, the presentation of the solution will be summarized.

2. BACKGROUND AND MATHEMATICS

Light is a transverse electromagnetic wave. The electric field intensity $\boldsymbol{E}$ is orthogonal to the magnetic flux density $\boldsymbol{B}$. Both $\boldsymbol{E}$ and $\boldsymbol{B}$ are orthogonal to the direction of propagation.

For a light wave traveling in the $+z$-direction, as in figure 2.1, the transverse requirement specifies that the fields have no dependence on x or y and are functions

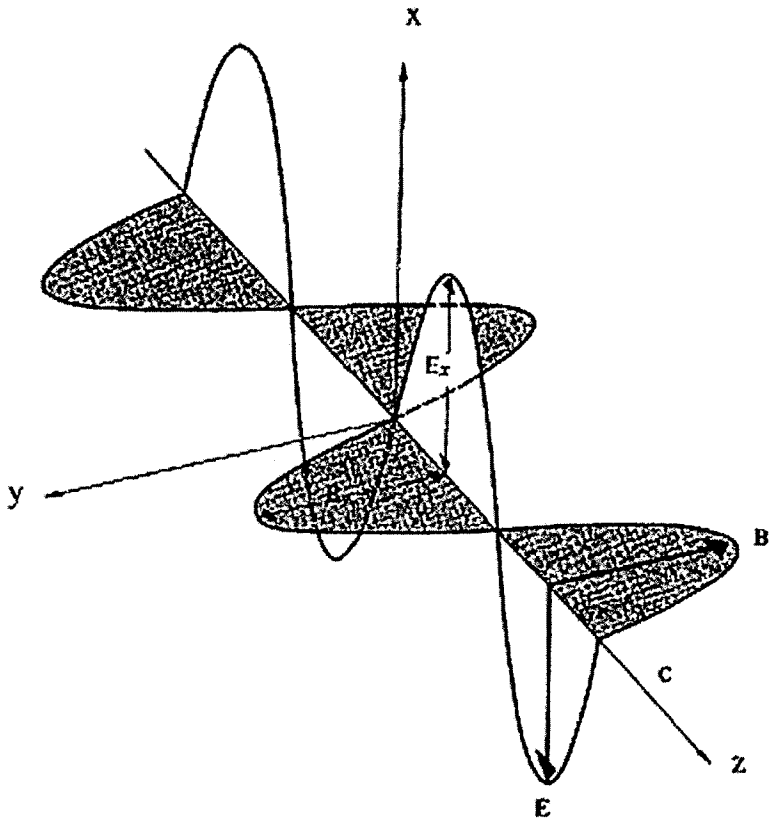

Fig. 2.1. Orthogonal harmonic components $\boldsymbol{B}-$ and $\boldsymbol{E}-$ fields in a transverse electromagnetic plane wave (Adapted from [5]).

of only z and t. Thus, Maxwell's Equations, listed in equation 2.1, are solved as equations of the form: $\boldsymbol{E}(x,y,z,t) = \boldsymbol{E}(z,t)$ and $\boldsymbol{H}(x,y,z,t) = \boldsymbol{H}(z,t)$.

$$\begin{aligned} \nabla \times \boldsymbol{E} &= -\mu \tfrac{\partial \boldsymbol{H}}{\partial t}, \\ \nabla \times \boldsymbol{H} &= \epsilon \tfrac{\partial \boldsymbol{E}}{\partial t}, \\ \nabla \cdot \boldsymbol{E} &= 0, \\ \nabla \cdot \boldsymbol{H} &= 0, \end{aligned} \tag{2.1}$$

where $\boldsymbol{H} = \frac{1}{\mu}\boldsymbol{B}$ is the magnetic field intensity. Then, assuming that $\boldsymbol{D} = \epsilon \boldsymbol{E}$ and $\boldsymbol{B} = \mu \boldsymbol{H}$, where $\boldsymbol{H}$ is propagating in the y-direction and $\boldsymbol{E}$ is propagating in the x-direction, the source-free Maxwell's equations become:

$$\begin{aligned} \hat{z} \times \tfrac{\partial \boldsymbol{E}}{\partial z} &= -\mu \tfrac{\partial \boldsymbol{H}}{\partial t}, \\ \hat{z} \times \tfrac{\partial \boldsymbol{H}}{\partial z} &= \epsilon \tfrac{\partial \boldsymbol{E}}{\partial t}. \\ \tfrac{\partial E_z}{\partial z} &= 0 \\ \tfrac{\partial H_z}{\partial z} &= 0 \end{aligned} \tag{2.2}$$

Taking the dot-product of Ampére's Law with the unit vector $\hat{z}$ and keeping in mind that $\hat{z} \cdot (\hat{z} \times \boldsymbol{A}) = 0$ yields:

$$\hat{z} \cdot \left(\hat{z} \times \frac{\partial \boldsymbol{H}}{\partial z} \right) = \epsilon \hat{z} \cdot \frac{\partial \boldsymbol{E}}{\partial t} = 0 \Longrightarrow \frac{\partial E_z}{\partial t} = 0.$$

It then follows that E_z and H_t are constants independent of z and t because $\partial_z E_z = 0$ and $\partial_z H_z = 0$, respectively. This means that the fields have components in only the x and y directions. Then the transverse electromagnetic fields describing the z-traveling wave can be written as in equation 2.3.

$$\begin{aligned} \boldsymbol{E}(z,t) &= \hat{x} E_x(z,t) + \hat{y} E_y(z,t) \\ &= \hat{x} E_x \cos(\omega t - kz + \phi_x) + \hat{y} E_y \cos(\omega t - kz + \phi_y) \\ \boldsymbol{H}(z,t) &= \hat{x} H_x(z,t) + \hat{y} H_y(z,t) \\ &= \hat{x} H_x \cos(\omega t - kz + \phi_x) + \hat{y} H_y \cos(\omega t - kz + \phi_y). \end{aligned} \tag{2.3}$$

where ω is the angular frequency, k is the propagation constant, and ϕ is the phase of the field. In the particular case of the wave shown in figure 2.1, $\boldsymbol{E}$ is oriented in

only the $\hat{x}$ direction and $\boldsymbol{H}$ is oriented in only the $\hat{y}$ direction, which allows further simplification of equation 2.3 when the specific waveform depicted by figure 2.1 is considered:

$$\begin{aligned} \boldsymbol{E}(z,t) &= \hat{x}E_x\cos(\omega t - kz + \phi), \\ \boldsymbol{H}(z,t) &= \hat{y}H_y\cos(\omega t - kz + \phi). \end{aligned} \tag{2.4}$$

Since the wave is traveling in the z-direction, $\boldsymbol{E}$ is propagating in the x-direction, and $\boldsymbol{H}$ is propagating in the y-direction, the relationship that $\boldsymbol{E} \times \boldsymbol{H} = \hat{k}$ is met because $\hat{x} \times \hat{y} = \hat{z}$. The remainder of the derivations will be made using only the electric field because the magnetic field contains redundant information [6].

The wave defined in equation 2.3 can be rewritten through use of Euler's Identity $e^{j\omega t} = \cos\omega t + j\sin\omega t$ as

$$\boldsymbol{E}(z,t) = Re[\boldsymbol{E}e^{j(\omega t+\phi)}] = Re[\boldsymbol{E}e^{j\phi}e^{j\omega t}]. \tag{2.5}$$

As is customary in phasor notation, the real part of equation 2.5 can be dropped and the $e^{j\omega t}$ can be suppressed to obtain [7]:

$$\boldsymbol{E}(z,t) = \hat{x}E_x e^{j\phi_x} + \hat{y}E_y e^{j\phi_y}. \tag{2.6}$$

The form for the electric field vector given in equation 2.6 is the phasor form and will simplify the upcoming discussions.

2.1 Polarization Ellipse

Begin with the phasor representation for $\boldsymbol{E}$ as given in equation 2.6. By restoring the factor $e^{j\omega t}$ the time-varying field is obtained:

$$\boldsymbol{E}(z,t) = (\hat{\boldsymbol{x}}E_x + \hat{\boldsymbol{y}}E_y)e^{j(\omega t-kz)}. \tag{2.7}$$

If $\boldsymbol{E}_x$ and $\boldsymbol{E}_y$ are replaced with polar forms $E_x = Ae^{j\phi_a}$ and $E_y = Be^{j\phi_b}$ respectively, the following is obtained:

$$\begin{aligned} \boldsymbol{E}(z,t) &= (\hat{\boldsymbol{x}}Ae^{j\phi_a} + \hat{\boldsymbol{y}}Be^{j\phi_b})e^{j(\omega t-kz)}, \\ &= \hat{\boldsymbol{x}}Ae^{j(\omega t-kz+\phi_a)} + \hat{\boldsymbol{y}}Be^{j(\omega t-kz+\phi_b)}. \end{aligned} \tag{2.8}$$

The polarization of the wave is the time-varying real-valued field $\boldsymbol{\mathcal{E}}(z,t) = Re[\boldsymbol{E}(z,t)]$ [6]. Extracting real parts and setting $\boldsymbol{\mathcal{E}}(z,t) = Re[\boldsymbol{E}(z,t)] = \hat{\boldsymbol{x}}\mathcal{E}_x(z,t) + \hat{\boldsymbol{y}}\mathcal{E}_y(z,t)$, the corresponding real-valued x and y components are found:

$$\begin{aligned} \mathcal{E}_x(t) &= A\cos(\omega t - kz + \phi_a), \\ \mathcal{E}_y(t) &= A\cos(\omega t - kz + \phi_b). \end{aligned} \tag{2.9}$$

Finally, to determine the polarization of the wave, consider the time-dependence of these fields at some fixed point along the z-axis. For example, let $z = 0$. Then,

$$\begin{aligned} \mathcal{E}_x(t) &= A\cos(\omega t + \phi_a), \\ \mathcal{E}_y(t) &= B\cos(\omega t + \phi_b), \end{aligned} \tag{2.10}$$

where the electric field vector $\boldsymbol{\mathcal{E}}(t) = \hat{\boldsymbol{x}}\mathcal{E}_x(t) + \hat{\boldsymbol{y}}\mathcal{E}_y(t)$ will be rotating on the xy-plane with angular frequency ω and its tip tracing an ellipse. This is seen by using trigonometric identities:

$$\begin{aligned} \mathcal{E}_x(t) &= A[\cos\omega t\cos\phi_a - \sin\omega t\sin\phi_a] \\ \mathcal{E}_y(t) &= B[\cos\omega t\cos\phi_b - \sin\omega t\sin\phi_b] \end{aligned} \tag{2.11}$$

to expand equation 2.10 and then solve for $\cos\omega t$ and $\sin\omega t$, leading to:

$$\begin{aligned} \cos\omega t\sin\phi &= \tfrac{\mathcal{E}_y(t)}{B}\sin\phi_a - \tfrac{\mathcal{E}_x(t)}{A}\sin\phi_b, \\ \sin\omega t\sin\phi &= \tfrac{\mathcal{E}_y(t)}{B}\cos\phi_a - \tfrac{\mathcal{E}_x(t)}{A}\cos\phi_b, \end{aligned} \tag{2.12}$$

where $\phi = \phi_a - \phi_b$ is defined to be the relative phase angle [8]. Now, if the sum of the squares of the two equations is found, a quadratic equation for the components $\mathcal{E}_x$ and $\mathcal{E}_y$ is obtained through use of the trigonometric identity $\sin^2\omega t + \cos^2\omega t = 1$, as in equation 2.13.

$$\left(\frac{\mathcal{E}_y(t)}{B}\sin\phi_a - \frac{\mathcal{E}_x(t)}{A}\sin\phi_b\right)^2 + \left(\frac{\mathcal{E}_y(t)}{B}\cos\phi_a - \frac{\mathcal{E}_x(t)}{A}\cos\phi_b\right)^2 = \sin^2\phi$$

which simplifies to:

$$\frac{\mathcal{E}_x^2}{A^2} + \frac{\mathcal{E}_y^2}{B^2} - 2\cos\phi\frac{\mathcal{E}_x\mathcal{E}_y}{AB} = \sin^2\phi. \tag{2.13}$$

Equation 2.13 is referred to as the polarization ellipse. Note that the various values of A, B, and ϕ lead to the polarization ellipse being an ellipse, circle, or a straight

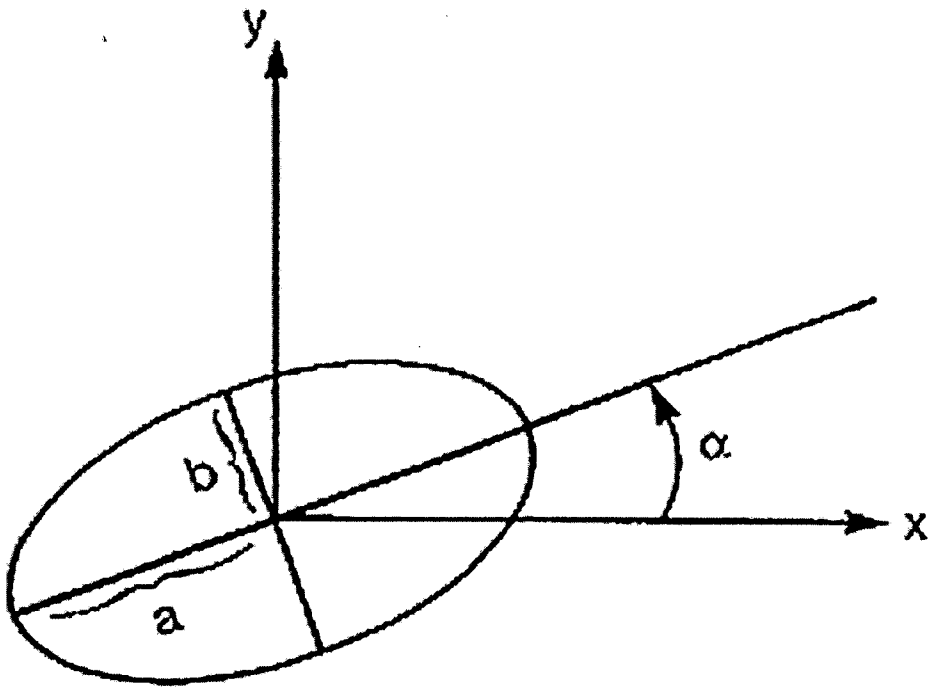

Fig. 2.2. The Polarization Ellipse [10].

line [9]. Thus, the electric field is referred to as elliptically, circularly, or linearly polarized. An example of the polarization ellipse is shown in figure 2.2.

The semi-major axis of the ellipse is a and the semi-minor axis is b with ellipticity $\frac{b}{a}$ and azimuth α. Figure 2.2 does not depict the handedness of the ellipse, which indicates whether the ellipse is traced out in a clockwise or counterclockwise direction.

2.1.1 Linear Polarization

Linear polarization is obtained when the phasor amplitudes are $\boldsymbol{E} = \hat{\boldsymbol{x}}A \pm \hat{\boldsymbol{y}}B$, which requires that $\phi = 0$ or $\phi = \pi$, and correspond to either $\phi_a = \phi_b = 0$ or the combination $\phi_a = 0$ and $\phi_b = -\pi$. In this case, equation 2.13 simplifies to:

$$\frac{\mathcal{E}_x^2}{A^2} + \frac{\mathcal{E}_y^2}{B^2} \mp 2\frac{\mathcal{E}_x \mathcal{E}_y}{AB} = 0 \Longrightarrow \left(\frac{\mathcal{E}_x}{A} \mp \frac{\mathcal{E}_y}{B}\right)^2 = 0$$

which represents straight lines defined as:

$$\mathcal{E}_y = \pm\frac{B}{A}\mathcal{E}_x.$$

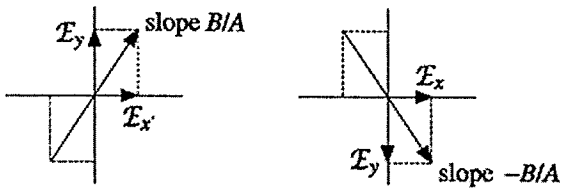

Then, the fields indicated by such a polarization ellipse in which $\phi = 0$ or $\phi = \pi$ take the forms:

$$\begin{aligned} \mathcal{E}_x(t) &= A\cos\omega t \\ \mathcal{E}_y(t) &= B\cos\omega t \end{aligned} \qquad \text{and} \qquad \begin{aligned} \mathcal{E}_x(t) &= A\cos\omega t \\ \mathcal{E}_y(t) &= B\cos(\omega t - \pi) = -B\cos\omega t \end{aligned}$$

2.1.2 Circular Polarization

Circular Polarization arises when $A = B$ and $\phi = \pm\frac{\pi}{2}$. The polarization ellipse in equation 2.13 simplifies to the equation of a circle:

$$\frac{\mathcal{E}_x^2}{A^2} + \frac{\mathcal{E}_y^2}{A^2} = 1$$

In circular polarization, the direction of rotation must be specified in conjunction to the direction of propagation. If $\phi_a = 0$ and $\phi_b = -\frac{\pi}{2}$, then $\phi = \phi_a - \phi_b = \frac{\pi}{2}$ and the phasor amplitude is $\boldsymbol{E} = A(\hat{\boldsymbol{x}} - j\hat{\boldsymbol{y}})$, then the fields corresponding to this polarization ellipse are

$$\begin{aligned} \mathcal{E}_x(t) &= A\cos\omega t \\ \mathcal{E}_y(t) &= A\cos(\omega t - \frac{\pi}{2}) = -A\sin\omega t \end{aligned}$$

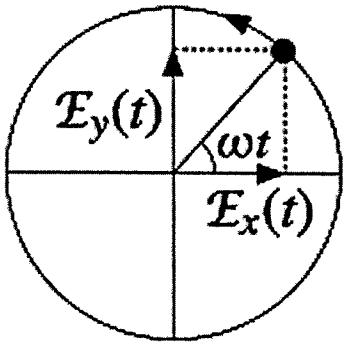

The wave is described as right-handed circular polarization if using the right hand as in the right-hand rule has the fingers of the right hand curling in the direction of rotation of the electric field when the thumb of the right hand is pointed in the direction of propagation.

Thus, for the example circular polarization states given in figure 2.3, the forward-moving field turning counterclockwise is right-handed circular polarization and the backward-moving field turning counterclockwise is left-handed circular.

Left-handed circular polarization arises from the case in which $\phi_a = 0$ and $\phi_b = \frac{\pi}{2}$. It leads to $\phi = \phi_a - \phi_b = -\frac{\pi}{2}$ and corresponding time-varying real-valued fields

$$\begin{aligned} \mathcal{E}_x(t) &= A\cos\omega t \\ \mathcal{E}_y(t) &= A\cos(\omega t - \frac{\pi}{2}) = -A\sin\omega t \end{aligned}$$

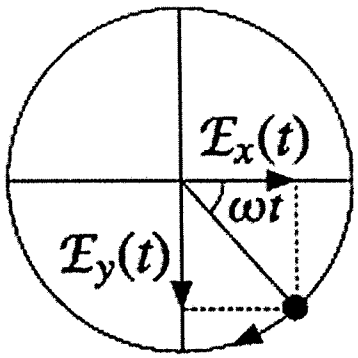

If the wave were traveling in the backwards-direction, however, it would be right-handed circular. Figure 2.3 shows the four cases that have arisen from this discussion of circular polarization.

Table 2.1

Mathematical representations of the four circularly polarized waves illustrated by figure 2.3

Polarization	**Movement**	**Expression in Phasor Form**
right-handed	forward	$\boldsymbol{E}(z) = A(\hat{\boldsymbol{x}} - j\hat{\boldsymbol{y}})e^{-jkz}$
left-handed	forward	$\boldsymbol{E}(z) = A(\hat{\boldsymbol{x}} + j\hat{\boldsymbol{y}})e^{-jkz}$
left-handed	backward	$\boldsymbol{E}(z) = A(\hat{\boldsymbol{x}} - j\hat{\boldsymbol{y}})e^{jkz}$
right-handed	backward	$\boldsymbol{E}(z) = A(\hat{\boldsymbol{x}} + j\hat{\boldsymbol{y}})e^{jkz}$

2.1.3 Elliptical Polarization

The general polarization case is that of elliptical polarization. First consider the special situation of elliptical polarization in which the phase difference is $\phi =$

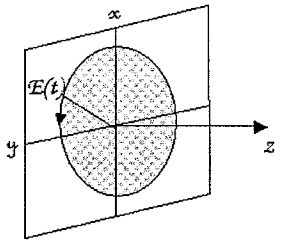

(a) right-polarized forward-propagating

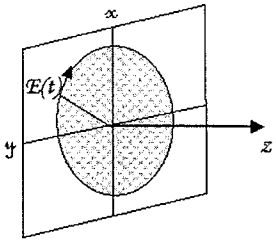

(b) left-polarized forward-propagating

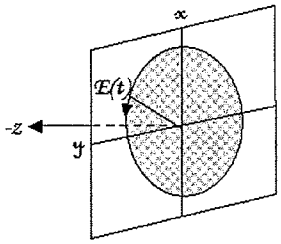

(c) left-polarized backward-propagating

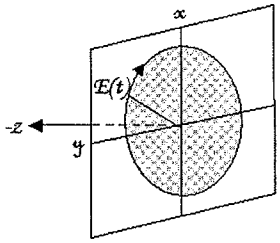

(d) right-polarized backward-propagating

Fig. 2.3. Four cases of left- and right-handed circular polarization [8].

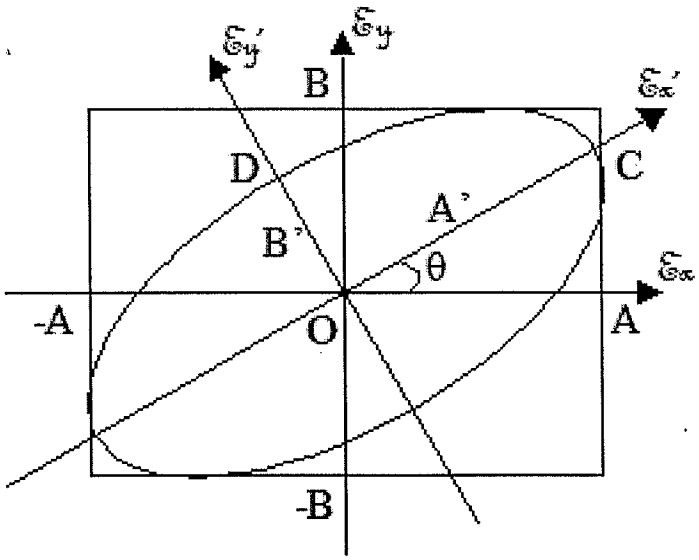

Fig. 2.4. General form of polarization ellipse [8].

$\phi_a - \phi_b = \pm\frac{\pi}{2}$ but $A \neq B$ in equation 2.13. With the semi-major and semi-minor axes oriented along the x and y directions, equation 2.13 reduces to the equation of an ellipse:

$$\frac{\mathcal{E}_x^2}{A^2} + \frac{\mathcal{E}_y^2}{B^2} = 1$$

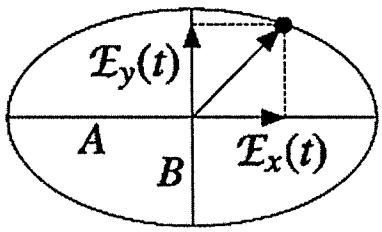

Note that if $A \neq B$ and ϕ is an arbitrary value, the major and minor axes of the ellipse will be rotated relative to the x and y directions. Hence, the general case of the polarization ellipse is reached. The figure above illustrates the general case [8].

To decide whether the polarization ellipse is left- or right- handed, the same procedure is followed as in the circular polarization case and will not be explained again here. However, the rotation around the polarization ellipse follows the general rule that the rotation is clockwise if the $\sin\phi < 0$ and counterclockwise if $\sin\phi > 0$ where $\phi = \phi_a - \phi_b$ [8].

2.2 Jones Matrix

Jones calculus is a methodical way of finding polarization states [10]. The phasor notation given of $\boldsymbol{E}$ in equation 2.6 can be rewritten in terms of the Jones vector as in equation 2.14.

$$\hat{\boldsymbol{s}}(z,t) = \begin{bmatrix} E_x e^{-j\phi_x} \\ E_y e^{-j\phi_y} \end{bmatrix} \tag{2.14}$$

where E_y is the magnitude and phase of the electric field in the $x-$direction and E_y is the magnitude and phase of the electric field in the $y-$direction. The assumption is made that the vector defined in equation 2.14 is normalized such that the magnitude is one, $E_x^2 + E_y^2 = 1$, and the electric field is standardized. Namely, $\phi = \phi_y - \phi_x$ where $\phi_x = \phi_a$ and $\phi_y = \phi_b$ in the polarization ellipse defined in equation 2.13.

Several examples of the Jones vector are given in table 2.2. The examples arise naturally from equation 2.13, table 2.1, and the discussions given in sections 2.1.3 and 2.1.1.

As mentioned previously, the Jones matrix is useful in keeping track of polarization states. It includes the transformation of light when it passes through a waveplate or a polarizer. A linear polarizer absorbs the orthogonal component and transmits light along the optical axis. As shown in figure 2.5, circularly-polarized incident light will be linearly-polarized after the light passes through a linear polarizer. The Jones matrix for a linear polarizer at an arbitrary rotation angle θ is

$$\begin{bmatrix} \cos\theta & -\sin\theta \\ \sin\theta & \cos\theta \end{bmatrix} \begin{bmatrix} p_x & 0 \\ 0 & p_y \end{bmatrix} \begin{bmatrix} \cos\theta & \sin\theta \\ -\sin\theta & \cos\theta \end{bmatrix} =$$

$$\begin{bmatrix} p_x\cos^2\theta + p_y\sin^2\theta & (p_x - p_y)\sin\theta\cos\theta \\ (p_x - p_y)\sin\theta\cos\theta & p_x\sin^2\theta + p_y\cos^2\theta \end{bmatrix} = \tag{2.15}$$

$$\begin{bmatrix} \cos^2\theta & \sin\theta\cos\theta \\ \sin\theta\cos\theta & \sin^2\theta \end{bmatrix}$$

Table 2.2
Jones vector representations of common polarization states [11] [4].

Polarization	(γ, Ψ)	**Jones Vector**
Linear horizontal	$\Psi = 0°$	$\begin{bmatrix} 1 \\ 0 \end{bmatrix}$
Linear vertical	$\Psi = 90°$	$\begin{bmatrix} 0 \\ 1 \end{bmatrix}$
Linear +45°	$(45°, 0)$	$\frac{1}{\sqrt{2}} \begin{bmatrix} 1 \\ 1 \end{bmatrix}$
Linear -45°	$(45°, 0)$	$\frac{1}{\sqrt{2}} \begin{bmatrix} 1 \\ -1 \end{bmatrix}$
Right-handed circular	$(45°, -\frac{\pi}{2})$	$\frac{1}{\sqrt{2}} \begin{bmatrix} 1 \\ j \end{bmatrix}$
Left-handed circular	$(45°, \frac{\pi}{2})$	$\frac{1}{\sqrt{2}} \begin{bmatrix} 1 \\ -j \end{bmatrix}$

when $p_x = 1$ and $p_y = 0$ which assumes that the retarder is aligned perfectly along the $x-$axis.

Lastly, the resulting polarization of an optical system can be obtained by multiplying the Jones vector for the system by the cascaded Jones matrices.

$$\begin{bmatrix} JonesMatrix \\ Element2 \end{bmatrix} \begin{bmatrix} JonesMatrix \\ Element1 \end{bmatrix} \begin{bmatrix} Jones \\ Vector \end{bmatrix} = \begin{bmatrix} Resulting \\ Vector \end{bmatrix} \tag{2.16}$$

2.3 Variable Waveplates

The variable waveplate is an important optical component in changing polarization. It is a birefringent material that changes the phase relationship between polarization components that are orthogonal to one another. The two orthogonal

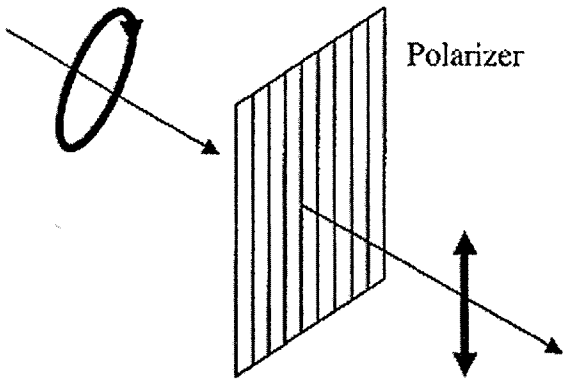

Fig. 2.5. Elliptical polarization is converted into linear polarization by a polarizer.

components are the basis for all types of polarization. The incoming light is broken into two rays called the extraordinary ray having index of refraction η_e and the ordinary ray having index of refraction η_o. The two rays are orthogonal to one another and thus have different velocities through the material. As a birefringent material is rotated in the plane of incidence, the ordinary ray remains stationary while the extraordinary ray traces a circle about it. The difference in the two indices of refraction is quantized in terms of birefringence $\triangle\eta$ where $\triangle\eta = \eta_e - \eta_o$.

In the specific case in which the net path difference between the two axes is $\frac{\lambda}{4}$, the material is said to act as a quarter wave-plate (QWP) at the wavelength λ. As shown in figure 2.6, a quarter wave-plate is used to convert from linearly polarized to circularly polarized light and from circularly polarized to linearly polarized light.

Finally, the Jones matrix can be used to describe a linear wave-plate as in the expression given by equation 2.17. It is seen by inspection that the effect of the linear wave-plate is to rotate the input vector to the frame of the retarder, assume

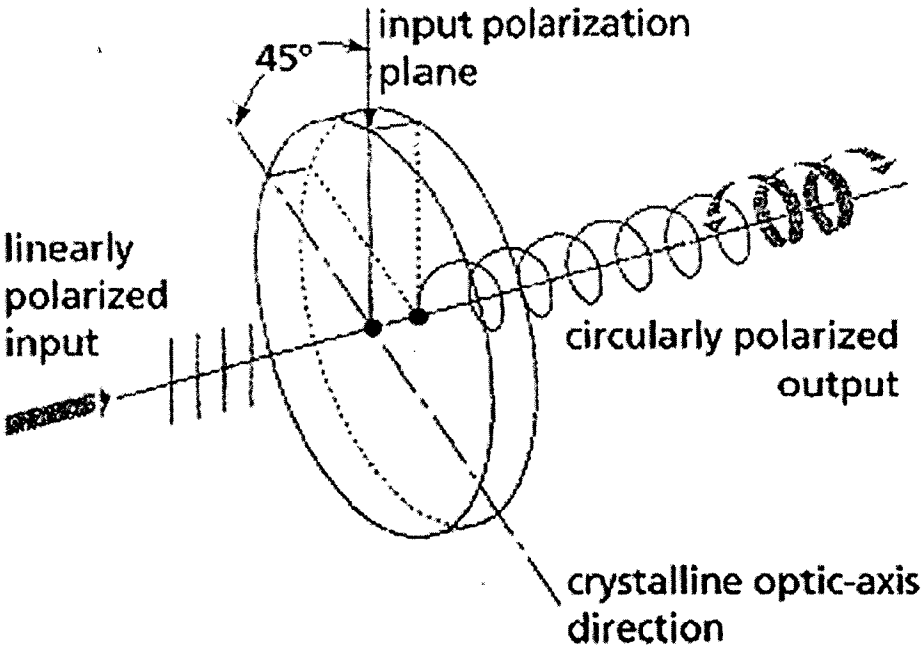

Fig. 2.6. If the QWP is aligned at 45°, the linearly polarized incident light is converted to circularly polarized light after passing through the QWP [12].

propagation through the retarder, and then rotate the input vector back to the original frame of reference.

$$\begin{bmatrix} \cos\rho & -\sin\rho \\ \sin\rho & \cos\rho \end{bmatrix} \begin{bmatrix} e^{\frac{i\zeta}{2}} & 0 \\ 0 & e^{\frac{-i\zeta}{2}} \end{bmatrix} \begin{bmatrix} \cos\rho & \sin\rho \\ -\sin\rho & \cos\rho \end{bmatrix} =$$

$$\begin{bmatrix} \cos\rho & -\sin\rho \\ \sin\rho & \cos\rho \end{bmatrix} \begin{bmatrix} \cos\rho e^{\frac{i\zeta}{2}} & \sin\rho e^{\frac{i\zeta}{2}} \\ -\sin\rho e^{\frac{-i\zeta}{2}} & \cos\rho e^{\frac{-i\zeta}{2}} \end{bmatrix} = \tag{2.17}$$

$$\begin{bmatrix} \cos^2(\rho)\, e^{-j\left(\frac{\zeta}{2}\right)} + \sin^2(\rho)\, e^{j\left(\frac{\zeta}{2}\right)} & -2j\cos(\rho)\sin(\rho)\sin\left(\frac{\zeta}{2}\right) \\ -2j\cos(\rho)\sin(\rho)\sin\left(\frac{\zeta}{2}\right) & \cos^2(\rho)\, e^{j\left(\frac{\zeta}{2}\right)} + \sin^2(\rho)\, e^{-j\left(\frac{\zeta}{2}\right)} \end{bmatrix}$$

where ρ is the angle of the fast axis of the wave-plate and ζ is the phase difference between the long and short paths [4].

3. FEMTOSECOND PULSE SHAPING

3.1 Basics

The available control electronics are too slow to modulate a laser pulse in the femtosecond time domain. Thus, the amplitude and phase of the laser field is modulated in the frequency domain. The time and frequency representation of a femtosecond laser pulse are connected by the Fourier transform [13].

Using the Fourier transform, the complex spectral intensity $\tilde{E}(\omega)$ can be described by

$$\tilde{E}(\omega) = \int_{-\infty}^{\infty} E(t) e^{-j\omega t} dt, \tag{3.1}$$

where $E(t)$ is the temporal electric field of the laser pulse. The electric field in the time domain $E(t)$ can be written using the inverse Fourier transform

$$E(t) = \frac{1}{2\pi} \int_{-\infty}^{\infty} \tilde{E}(\omega) e^{j\omega t} dt. \tag{3.2}$$

The complex quantity $\tilde{E}(\omega)$ has values for both positive and negative frequencies. Thus, the following quantities are introduced:

$$\tilde{E}^{+} = \frac{1}{2\pi} \int_{0}^{\infty} \tilde{E}(\omega) e^{j\omega t} dt, \tag{3.3}$$

$$\tilde{E}^{-} = \frac{1}{2\pi} \int_{-\infty}^{0} \tilde{E}(\omega) e^{j\omega t} dt, \tag{3.4}$$

where both equations 3.3 and 3.4 are complex quantities. Note, however, that the values $\tilde{E}^{-}$ and $\tilde{E}^{+}$ are not measurable and do not have a physical meaning. The original electric field can be reconstructed from equations 3.3 and 3.4

$$E(t) = \tilde{E}^{+} + \tilde{E}^{-}, \tag{3.5}$$

where it is assumed that there is no loss of resolution due to the Nyquist effect.

Table 3.1

Mathematical descriptions of a laser pulse and the corresponding electric field expression. The time-bandwidth product is also given for each of the spectral shapes [13] in addition to the FWHM deconvolution factor [14].

Function	**E(t)**	**K**	**FWHM Deconvolution Factor**
Gaussian	$e^{-\frac{1}{2}\left(\frac{t}{t_0}\right)^2}$	0.441	$\sqrt{2}$
Hyperbolic secant	$\frac{1}{cosh\left(\frac{t}{t_0}\right)}$	0.315	1.543
Lorentz	$\frac{1}{\left[1+\left(\frac{t}{t_0}\right)\right]^2}$	0.142	0.450

Since it is experimentally easier to measure half-maximum quantities, the relationship between the duration and spectral bandwidth of the laser pulse can be written as

$$\triangle\nu\triangle t = K, \tag{3.6}$$

where $\omega = 2\pi\nu$ and $\triangle\nu$ is the frequency bandwidth full-width at half-maximum (FWHM), $\triangle t$ is the FWHM in the time domain, and K is the time-bandwidth product for the specific shape of the waveform (see Table 3.1).

In order to generate a laser pulse that is short in the time domain, a broad spectral bandwidth needs to be used. This introduces a Fourier-transform-limited pulse, also known as just a transform-limited pulse. The minimum time duration of a pulse is

$$\triangle t = K\frac{\lambda_0^2}{\triangle\lambda \cdot c}, \tag{3.7}$$

where $\triangle\lambda$ is the spectrum FWHM (nm), λ_0 is the central wavelength (nm), and c is the speed of light (m/s) [13].

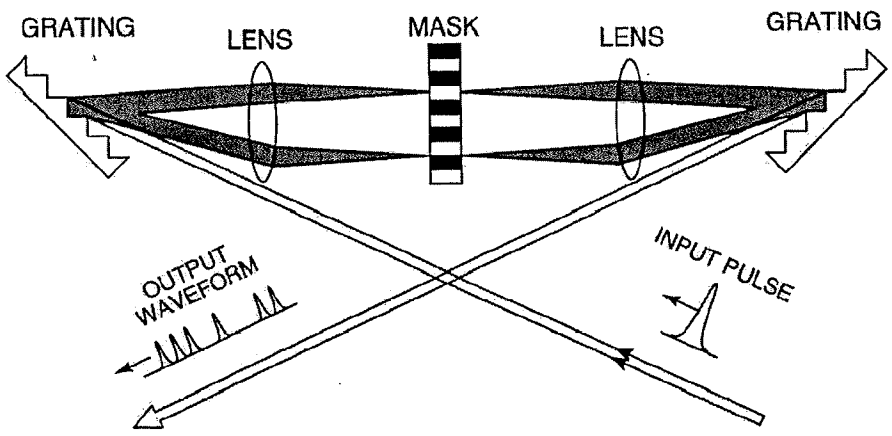

Fig. 3.1. Two-pass pulse shaper design. [15]

3.2 Fourier Transform Pulse Shaping

Fourier transform pulse shaping has been used to generate arbitrary optical pulses [15]. In addition, liquid crystal modulators have been used to provide programmable femtosecond optical pulse shaping [16–21]. Initially, a basic Fourier transform femtosecond pulse shaping apparatus was utilized as a transmission system with two diffraction gratings, two achromatic lens, and a mask [15]. As indicated by Figure 3.1, a free-space input pulse is diffracted off of the first reflective diffraction grating causing individual frequency components to spread. The first lens then takes the Fourier transform of each of the angularly separated components. Next, a spectral phase and amplitude are applied to each of the frequency components by the LCM. The system is completed by the inverse Fourier transform being taken by the second lens and the recombination of the frequency components by the final reflection diffraction grating.

It is important to note that the output waveform would be identical to the input pulse if the mask were not present because the gratings are simply separating or recombining the different frequency components and the lens are just taking the Fourier or inverse Fourier transform of each of the frequency components (refer to

Section 3.1). This reveals a crucial point. The system is free of dispersion in the absence of the mask.

3.3 Reflection Geometry

Instead of using the additional achromatic lens and reflective diffraction grating, as used in previous examples, a mirror can be placed so the light passes twice through the system. This method, reflection geometry Fourier transform pulse shaping, uses the polarizer at the entrance face of the unit to act as a polarizer for both the light entering and leaving the LCM. It also allows for lower loss and ease in alignment (see section 3.6). Applying the Fourier transform reflection geometry, this feature doubles the action of the SLM, resulting in a faster time response between switching the drive settings and the allowance of greater phase modulation [22].

In the previous set of experiments, a reflection geometry Fourier transform pulse shaper was utilized [4]. This method maintains the characteristics of the transmission Fourier transform pulse shaper (refer to section 3.2), but with a few changes. Since the mirror is located at the beam waist, the mask is moved slightly out of focus and operates on frequency spots that are not truly at their minimum. In the previous set of experiments, this effect was negligible because the mask was close to the mirror relative to the lens focal length. This will be discussed in detail in section 4.2. Figure 3.2 shows that the setup for the reflective Fourier transform pulse shaper in the previous set of experiments has an identical design to that of the transmission Fourier transform pulse shaper.

The design indicated by figure 3.2 also shows the bidirectional collimator and the circulator, which will be discussed in sections 3.4.3 and 3.4.2, respectively.

3.4 Optical Components

When the optical components are selected for the system, initial pulse shaping considerations are required. First and foremost, the beam input size on the grating

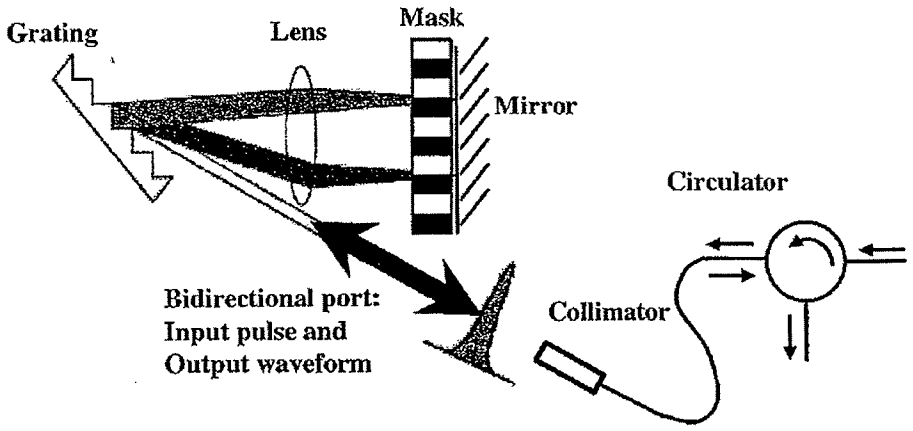

Fig. 3.2. Reflective pulse shaper used in two-layer system.

must be determined and the focal length of the lens must be selected. The function and selection considerations of each of the optical components will now be discussed in detail, beginning with the polarization controller, fiber circulator, collimator, grating, lens, and mirror. The different components of the two-layer LCM system and the single-layer LCM system will then be explained. Finally, the component selection will be discussed.

3.4.1 Polarization Controller

The polarization of the transmitted light in single mode fiber is altered by a polarization controller. The FPC Series of Polarization Controllers (PC), used in the set of experiments described by this thesis, create three independent 'wave plates' $\left(\frac{\lambda}{4}, \frac{\lambda}{2}, \frac{\lambda}{4}\right)$ which, together, convert elliptical polarization into linear polarization through use of stress-induced birefringence. The mathematics involved were explained in section 2.3. Figure 3.3 shows the polarization states, which are referred to by their shape when projected onto the plane of propagation.

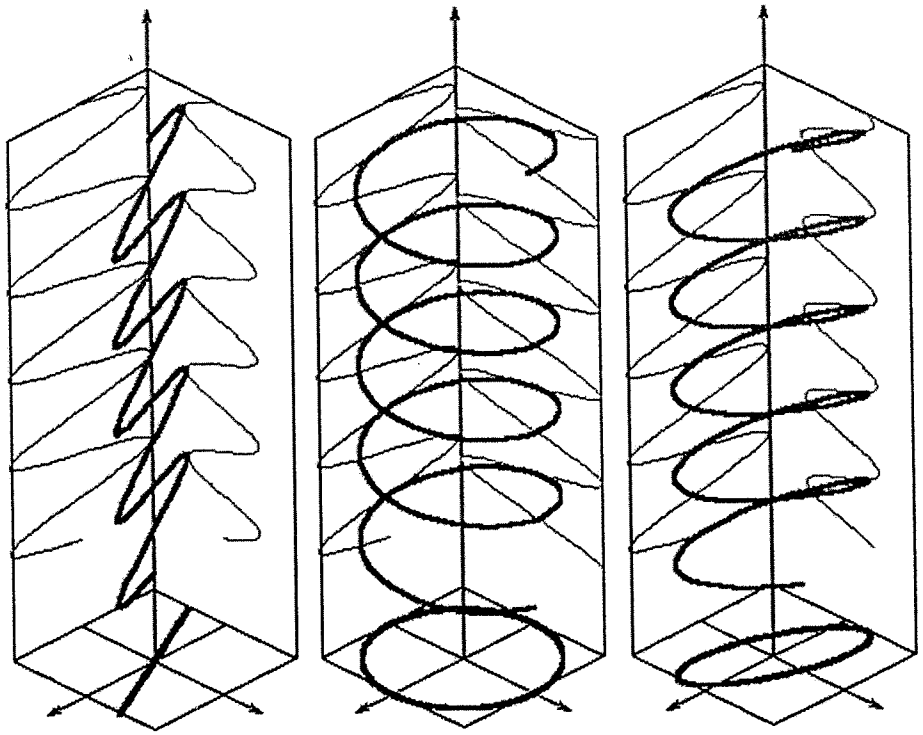

Fig. 3.3. Sample polarization state illustrations. The signal polarization is referred to by the projection onto the plane of propagation.

3.4.2 Fiber Circulator

A circulator is a device that allows the light to enter and leave the system through a single signal terminal. Physically, the circulator is packaged in a cylindrical tube about 6 cm long and 2 cm in circumference. A schematic for a fiber circulator is shown in figure 3.4.

The light goes from port one to port two and from port two to port three with very little loss. The circulator used for this set of experiments has a measured insertion loss from port one to port two of 0.60 dB and from port two to port three of 0.73 dB. The insertion loss from port three to port two and from port two to port one are on the order of 50 dB, so it has been assumed that no light passes in that direction. Thus, the circulator contributes to a loss of 1.43 dB within the entire system.

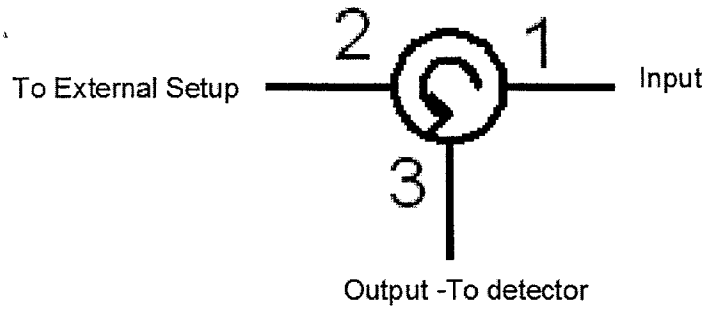

Fig. 3.4. Schematic of fiber circulator. Low loss is present in passing from port one to port two or from port two to port three, but very high loss exists in the opposite direction.

3.4.3 Bidirectional Collimator

The bidirectional collimator performs an essential function within the pulse shaper. It ensures that the optical signal is incident upon the reflective diffraction grating in such a manner that a clear image is obtained by allowing only those components of the pulse traveling parallel to each other pass into free space. An angled body on the collimator minimizes the back reflection.

3.4.4 Reflective Diffraction Grating

The light in the collimated beam is spatially separated by wavelength upon incidence of the low PDL reflective diffraction grating. The selected grating for this set of experiments has 1100 $\frac{grooves}{mm}$ over an area of 2.5 cm $\times$ 2.5 cm on a substrate that is 0.6 cm thick. This grating was chosen because it was readily available.

First consider the microscopic view of a grating as depicted in figure 3.5, where α is the angle of the incident light with respect to the grating normal, β_0 is the angle of the zero-order reflected light with respect to the grating normal, β_{-1} and β_1 are the angles of the -1 and $+1$ orders of diffracted light, respectively, and d is the distance between grooves on the grating.

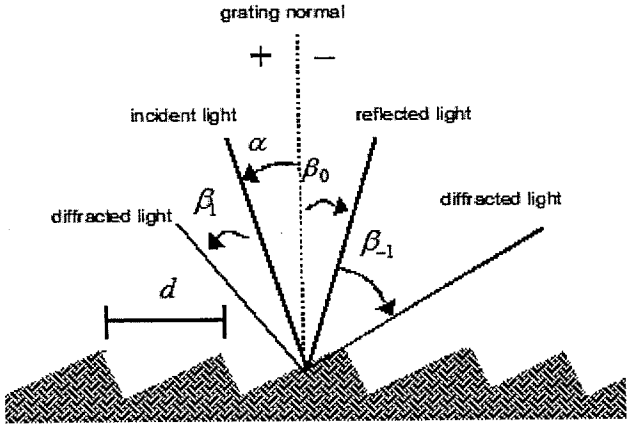

(a) Grating microscopic view showing the diffracted beam locations with respect to the incident angle and the grating normal.

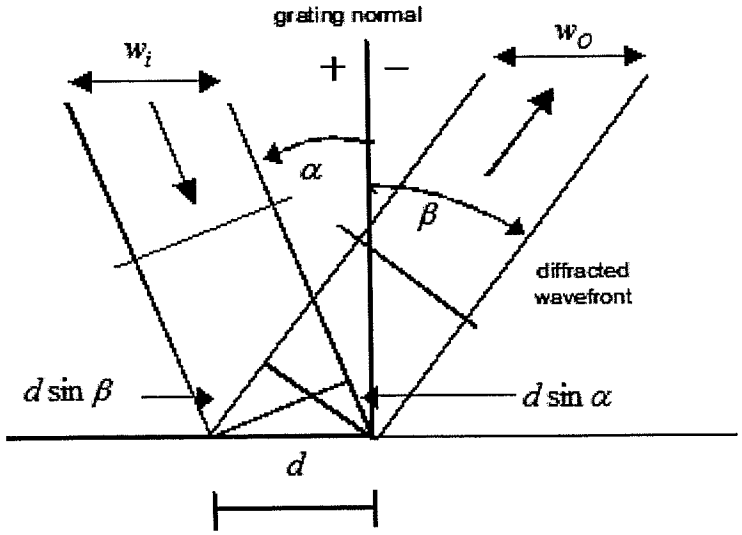

(b) Microscopic view of a grating showing the beam widths upon incidence and diffraction.

Fig. 3.5. Grating Microscopic Views.

Angular dispersion of the light can be calculated by beginning with the grating equation [23]:

$$m\lambda = d(\sin\alpha + \sin\beta), \tag{3.8}$$

where m is the diffraction order, λ is the wavelength, and d is the spacing between the grooves, as shown in figure 3.5. For a particular wavelength λ, all values of m for which $|\frac{m\lambda}{d}| < 2$ are realizable. However primary focus is placed on the first order diffraction because it generates the most power within the system.

For a given wavelength λ, ratio of the output beam width to the input beam width must be considered [23]. The effective magnification of the grating is

$$\frac{b}{a} = \frac{\cos\beta}{\cos\alpha}. \tag{3.9}$$

Different wavelengths within the incident waveform are incident upon the grating at the same angles but they diffract at different angles. Thus, while α is consistent for each of the wavelengths in the incident waveform, β is dependent on λ and the magnification described by equation 3.9 varies with wavelength. The ratio $\frac{b}{a}$ is also called the anamorphic magnification because it depends only on the angular configuration.

3.4.5 Achromatic Lens

An achromatic lens is a combination of lenses made from materials of different refractive indexes. They are constructed in a manner that the light entering the lens is focused (imaged) at a distance one focal length away on the other side of the lens.

Keeping in mind that the focal length of the lens must also coincide with the specifications of the grating, equation 3.9 must be modified. The following relationships can be defined [24]:

$$w_f = \frac{f\lambda}{\pi w_b}, \tag{3.10}$$

and

$$w_b = \frac{w_a \cos\beta}{\cos\alpha}, \tag{3.11}$$

where w_f is the beam radius at the focal plane, $w_a = \frac{1}{2}w_i$ is the beam radius at the grating incidence and $w_b = \frac{1}{2}w_0$ is the beam radius after reflection from the grating, as shown in figure 3.5. Combining equations 3.10 and 3.11, the overall beam radius at the focal plane is

$$w_f = \frac{\lambda f \cos\alpha}{\pi w_a \cos\beta}. \tag{3.12}$$

For convenience, define the beam diameter at the LCM plane to be the resolution. A detailed discussion of the pulse shaper resolution will be given in section 4.3.2.

Fixing the input angle while differentiating the output angle as a function of λ, the grating equation (equation 3.8) becomes [25]:

$$\cos\beta = \frac{mf}{d}\frac{\triangle\lambda}{\triangle x}. \tag{3.13}$$

where $\triangle x$ is the LCM pixel aperature. From this, the spectral range $\triangle\lambda$ can be calculated by

$$\frac{\triangle\lambda}{\triangle x} = \frac{d\cos\beta}{f}. \tag{3.14}$$

The spectral range will be revisited in section 3.5, where the component selection is discussed.

3.4.6 Gold Mirror

The gold mirror has a simple but important purpose. It is a single-layer polarization insensitive component that reflects the signal back through the shaper so an output signal can be obtained. The reflectance of the CVI 2.5 cm diameter gold mirror used in the experiments was 98%. A mirror with a higher reflectance could have been used but it would need to be used in a manner that ensures normal incidence and polarization insensitivity.

3.4.7 Liquid Crystal Modulator Basics

Liquid crystals (LCs) are a set of crystals that act as a single waveplate. A single crystal is a thin molecule that is about five times longer than it is wide [26].

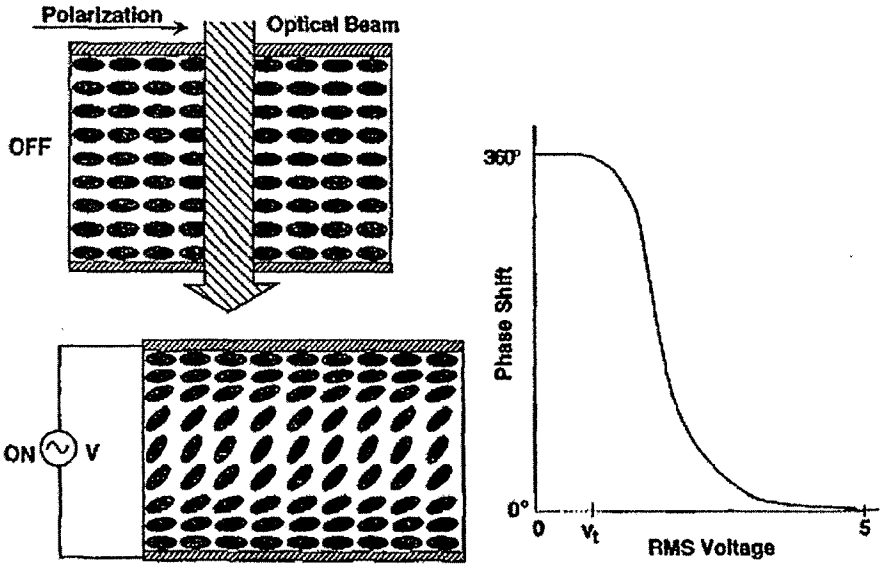

Fig. 3.6. Liquid crystal phase shift.

Application of a low voltage on the order of $1 - 10$ volts causes the LCs to reorient. The reorientation causes a change in the phase of the signal, as shown in figure 3.6.

3.4.8 Two-layer Liquid Crystal Modulator

The two-layer liquid crystal modulator (LCM) is a commercially available device that consists of two arrays of 128 rectangular electrodes, or pixels, each. The arrays are separated by a width of 2.2 mm. Each pixel can be controlled independently. Figure 3.7 shows front and side views of the liquid crystal modulator.

The pixels are a thin film of indium tin oxide (ITO). They are transparent for the spectral range of interest. Figure 3.8 shows the mask aperture layout.

Liquid crystals have no defined distance between the molecules as in an ordinary crystal. As depicted by figure 3.9, in the absence of an electric field, the crystals are aligned with their long axes along the horizontal direction.

When the voltage V is applied on the liquid crystal in the z-direction, electric dipoles are induced. The electric forces tilt the liquid crystal pixels along the z-

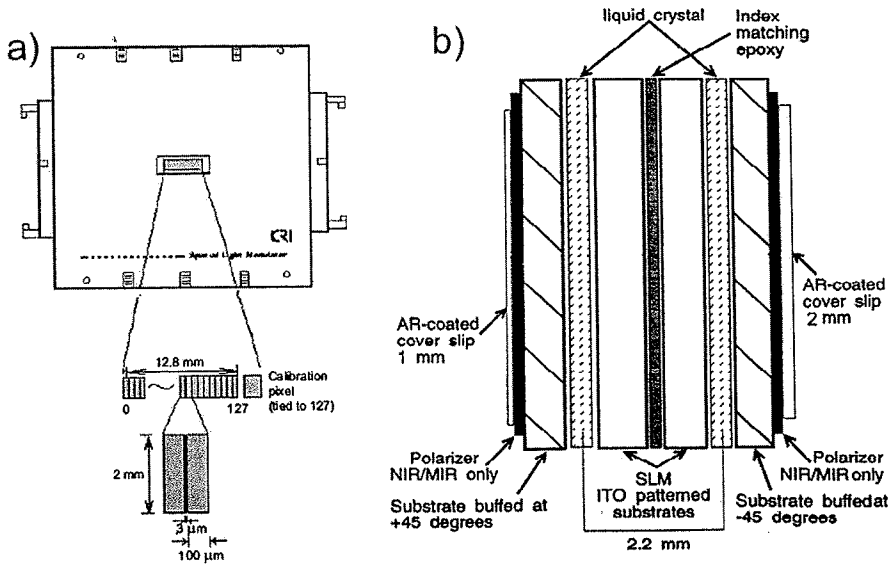

Fig. 3.7. Layout of two-layer LC array showing (A) the front view and (B) the side view [15].

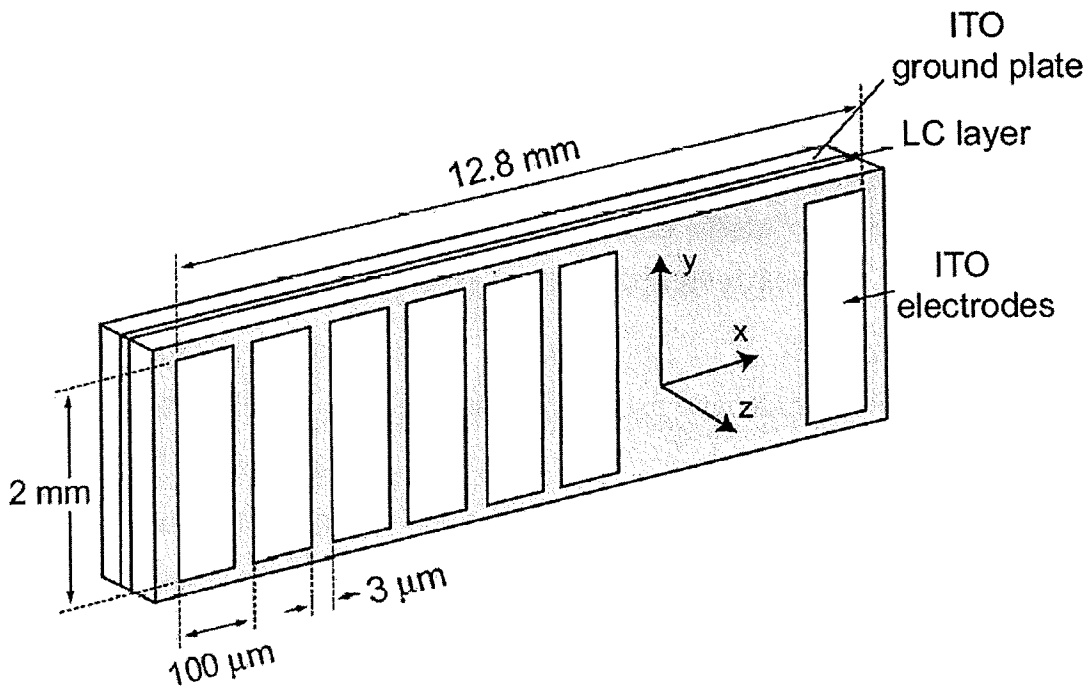

Fig. 3.8. Aperature mask layout on two-layer LC array [15].

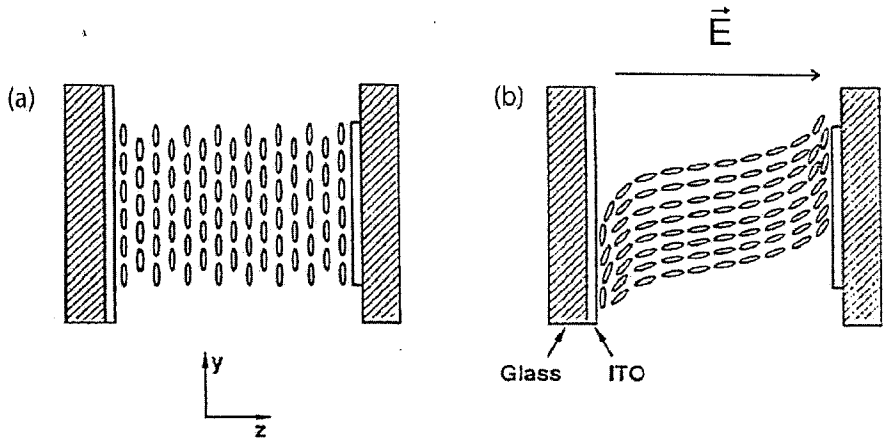

Fig. 3.9. In the absence of an applied electric field, LCs are directed with their long axes in the horizontal direction [15]

axis, which causes a change in the refractive index of the y-polarized light (adapted from [15]), and thus a change in the phase of the output wave. The x-component of the E-field does not experience a phase change. This means that the voltage changes the birefringence of the liquid crystal cell. For appropriate input polarization, the change in birefringence gives a change in the output polarization, which can be converted to an amplitude change through use of an output polarizer.

The input to the LCM controller is a voltage 'level' from $1 - 4096$ on each layer which correspond to nominal applied voltages of $0 - 10$ V. These 'levels' create the desired phase shift from $0 - 2\pi$ after passing through each of the pixels. Since a given voltage 'level,' applied through an external electronics LCM controller connected to the mask via ribbon cables is not a constant, it is necessary to calibrate the LCM prior to initial use.

3.4.9 Single-layer Liquid Crystal Modulator

The single-layer LCM operates the same way as the two-layer LCM, but without the added phase implied by the second layer, which is compensated by the quarter

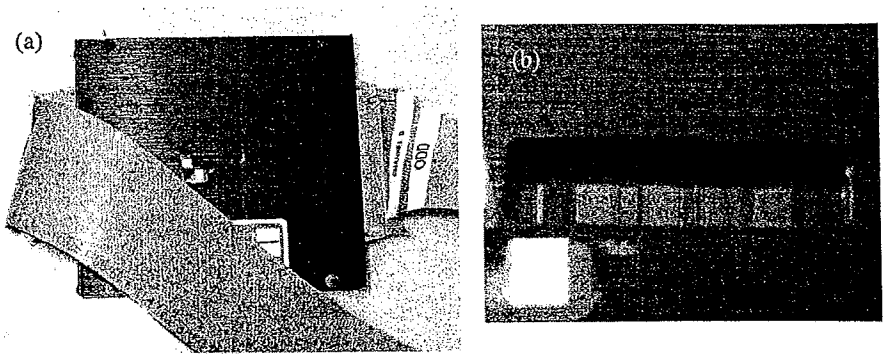

Fig. 3.10. Single-layer LCM photographs showing (A) the LCM and control cables and (B) a close view of the aperature showing lines of a programmed mask. [4].

wave-plate. The mathematics of this combination will be discussed in section 4.3.1. A single layer LCM and the connected cables are shown in figure 3.10. As with the two-layer LCM, the external electronics apply a given voltage 'level' to the mask via the ribbon cables. The voltage 'level' once again does not create the same phase shift on every pixel, so the LCM must be calibrated prior to inital in order to generate the phase shift from $0-2\pi$ is applied with known voltage 'level' values from $1-4096$ that, once again, correspond to nominal applied voltages of $0-10$ V.

3.5 Component Selection

As indicated by equations 3.12 and 3.14, spectral range $\triangle\lambda$ and resolution are dependent on grating spacing d and beam diameter at the grating incidence w_i. A narrow spectral range $\triangle\lambda$ and narrow beam diameter $2w_f$ incident on the LCM plane are desired for a practical application. Consequently, a smaller d and larger w_i are desired (refer to equations 3.14 and 3.12, respectively).

A grating with 1100 lines/mm was chosen because it is readily available commercially for the L-band communication wavelengths and the laser outputs at 1578 nm, which is in the center of the L-band. The collimator beam radius w_i cannot

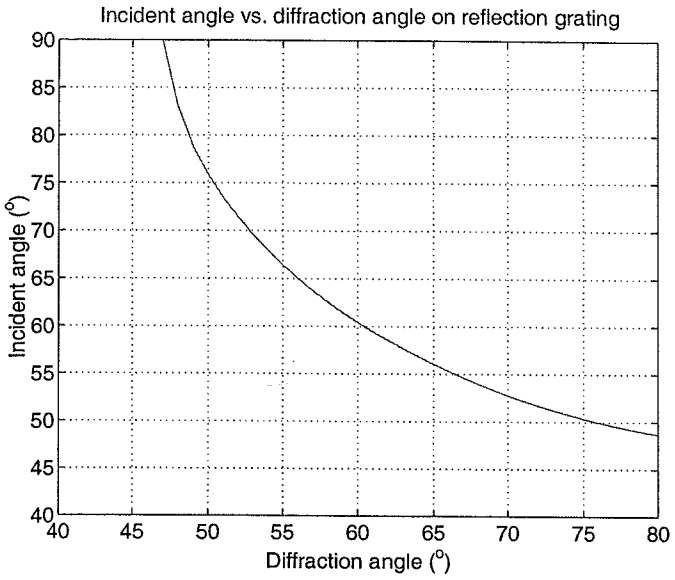

Fig. 3.11. Incident angle vs. diffraction angle at 1578 nm center wavelength based on the grating equation. [25]

be arbitrarily increased to improve resolution because increasing w_i results in an increased loss within the system. The lens focal length f and the grating diffraction angle β are additional design parameters [25].

Figure 3.11 shows the incident angle α versus diffraction angle β based on the grating equation (equation 3.8). Note that while the incident angle and diffraction angle can be increased arbitrarily in the theoretical calculations presented in figure 3.11, the grating is designed with the goal of an incident angle α and a diffracted angle β approximately equal to one another ($\alpha \approx \beta$). Also note that an excessively large incident or diffracted angle could result in unexpected effects such as higher order dispersion. It is recommended to maintain a diffraction angle on the grating in the range of $49^o - 55^o$ which corresponds to an incident angle of $77^o - 66^o$ at a center wavelength of 1578nm.

The laser outputs a nominal pulse width of 70 fs, which corresponds to a spectral FWHM of 60 nm centered at 1578nm. The setup requires a spectral range of twice the FWHM of the spectrum (120 nm). The focal length of the lens was selected

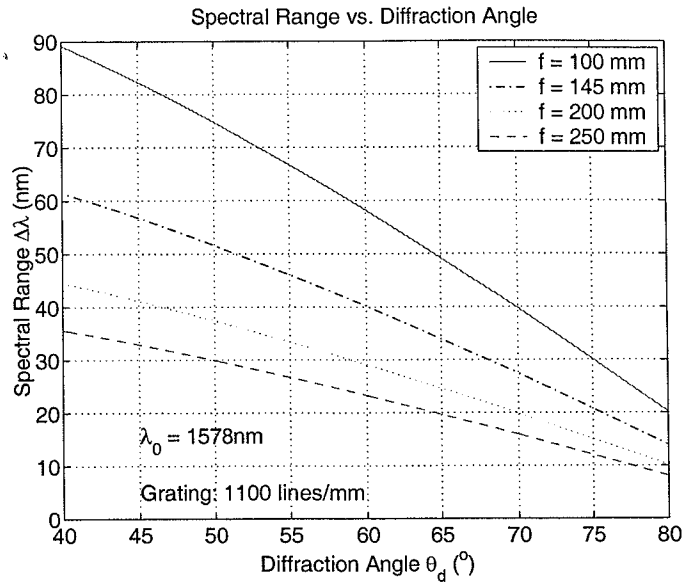

Fig. 3.12. Spectral Range as a function of diffraction angles off the grating.

between f = 100 mm, 145 mm, 200 mm, and 250 mm. Figure 3.12 shows the relationship between the spectral range and the diffraction angle for these lens for an LCM aperature of 12.8 mm, as defined by equation 3.14. The following observations need to be made. The spectral range is dependent upon the diffraction angle, but it is not as sensitive to diffraction angle as it is to the focal length of the lens. Diffraction angle must stay in the above specified range, and cannot be larger than 70^o. Higher resolution requires a smaller diffraction angle. Increasing the focal length of the lens to improve the spectral range requires more physical space for the pulse shaper system and also degrades resolution so a lens is selected in the mid-range of the investigated focal lengths.

The next component selected was the collimator. According to measurements taken of each of the collimators readily available in the lab, the collimator had to be selected from a beam width of 1.9 mm, 2.7 mm, 4.0 mm, or 5.4 mm. For this experiment, a collimator of 1.9 mm beam width was selected. Physically, the collimator is packaged in a cylindrical tube about 2 cm long and 2.5 cm in circumference.

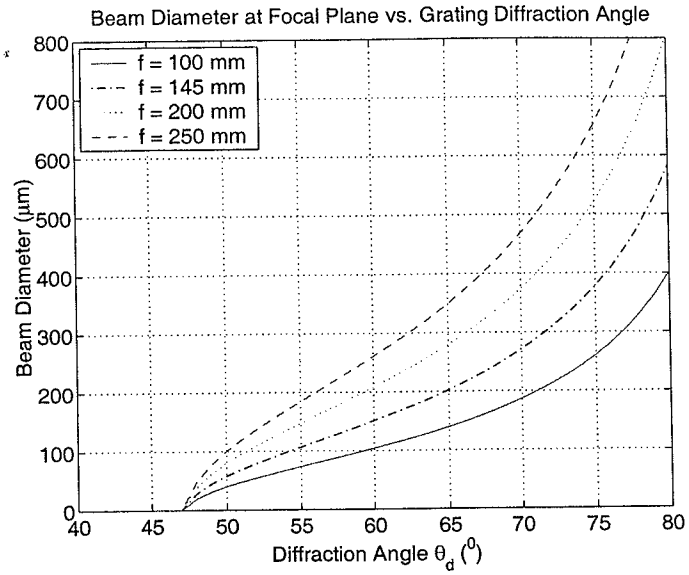

Fig. 3.13. Beam size as a function of diffraction angle off the grating.

After selection of the collimator, the lens was chosen. Figure 3.13 shows the beam size incident on the LCM plane for the lens of focal length $f = 100$ mm, 145 mm, 200 mm, and 250 mm. Figure 3.12 shows the relationship between the spectral range and the diffraction angle, as defined by equation 3.12. Note that a fundamental apriorism has been made in that the reflective mirror and LCM layer are close enough to one another that both are located at the beam waist. This assumption will be elucidated in section 4.3.2. The lens chosen had a focal length of $f = 145$ mm in order to achieve a resolution of 100μm while maintaining the diffraction angle in the range of $49^o - 55^o$.

At this point, all components were selected. Table 3.2 summarizes the components chosen for the system, including physical notes about the particular components.

Table 3.2: Specifications for each of the components selected for the polarization insensitive pulse shaper system, including the vendor, part number, physical attributes, and application to the system.

Component	**Vendor**	**Part Number**	**Physical Attributes**	**System Use**
PC	ThorLabs	FPC561	Operating Range 1310-1550nm, 12.7 × 2.50 × 3.65 in.	Adjust system input polarization from circular to linear. Also used to confirm polarization insensitivity.
Circulator	JDS Uniphase	CIR-330031000-001	$47mm \times 5mm$ with appx. one meter fiber at each port.	Allow the light to enter and leave the system through a single terminal.
Collimator	OFR	CFS-TA-11-1550	$1.9mm$ beam diameter output with appx. packaging of $7.9mm$ diameter and $21mm$ beam width. Angled body to minimize reflection.	Allow the passage of a collimated beam into and out of free space.
Grating	Richardson	3309FL-660	Reflection with 1100 lines/mm, 1" wide × 1" long	Spatially separate collimated beam by wavelength.
Lens	ThorLabs	AC254-145-C	$f = 145mm$, ACHR $1.55\mu m$	Focus the spatially separated light.
2-layer LCM	CRI	SLM-128-D-NM	$12.8mm(w) \times 5mm(h)$ Aperature with 128 pixels of $98\mu m \times 5mm$	Take FT/IFT of signal

Continued on next page.

Component	Vendor	Part Number	Physical Attributes	System Use
1-layer LCM	CRI	SLM-128-P-NM	$12.8mm(w) \times 5mm(h)$ Aperature with 128 pixels of $98\mu m \times 5mm$	Take FT/IFT of signal
Wave-plate	ThorLabs	WPQ05M-1550	1" diameter × 2.5 mm thick	Change signal polarization by $\frac{\lambda}{4}$ per pass.
Gold mirror	CVI	PG-PM-1037-C	1" diameter and 0.375" thickness.	Retro-reflect the signal so IFT can be taken.

3.6 Alignment of Pulse Shaper

The optical beam is in the infrared (IR) frequency range so an IR card was required to visually inspect the alignment of the pulse shaper. It was necessary to dim lights in the room in order to see the signal incident on the IR card. Also, the beam was confirmed to maintain a common height after each component and the system was designed so the incident and diffracted angles were less than 70^o, as discussed in section 3.5. Before performing the alignment procedure, the lengths of all fiber in the system were measured, including the polarization controller and circulator lengths from terminal one to terminal two and from terminal two to terminal three.

Ensuring low loss and quality output from the reflective pulse shaper was straightforward through the following alignment procedure:

1. The collimated beam was aligned so that it was propagating in a plane parallel to the optical table surface. The near- and far-fields were checked.

2. The diffraction grating was aligned in a plane normal to the optical table. There are three adjustments on the grating mount. The vertical height was first adjusted based on the grating first-order reflective beam. Next, the rotation

on the diffracted height was fine-tuned. Finally, the height was confirmed to be correct at a distance.

3. The lens was inserted one focal length from the grating. The wave was confirmed to be centered on the lens.

4. The gold mirror was inserted two focal lengths away from the grating and one focal length away from the lens. Using a CW source, the light was confirmed to reflect back into the center of the lens. When the mirror was adjusted so that the incident light was normal to the mirror surface and the distance from the mirror to the lens was one focal length, the output power through terminal three of the circulator was maximized.

5. Once each of the components were inserted into the shaper, the horizontal control on the grating was slightly adjusted to create the maximum symmetry possible in the output pulse.

6. Finally, the LCM (two-layer system) or QWP/LCM combination (one-layer system) was inserted into the pulse shaper apparatus.

It is necessary for the LCM, lens, and reflective mirror to be clean over the entire spectral range because of the spatial spreading of the spectrum. When the system was not in use, the grating was covered to maximize the lifetime in which the grating is clean and useful within the pulse shaper apparatus.

3.6.1 Insertion of Two-layer LCM

The LCM was inserted after the pulse shaper was aligned. The two-layer LCM was inserted as close to the mirror as physically possible. A translation stage assisted the process by minimizing the possibility of interfering with the alignment of the mirror. Next, the reflective mirror adjustment was revisited to confirm that the mirror was still aligned as desired.

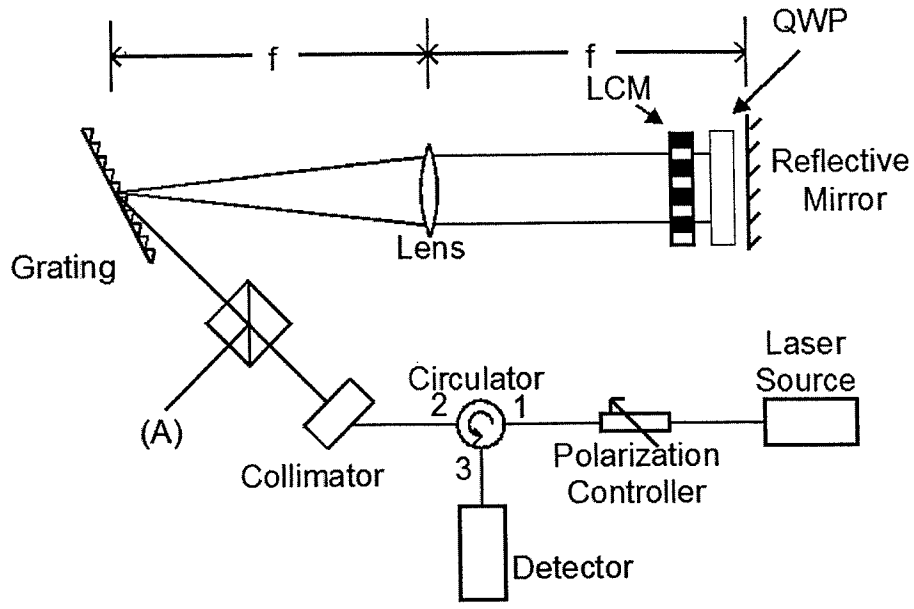

Fig. 3.14. A polarizing beam splitter was inserted into the pulse shaper immediately after the collimator to assist in the QWP alignment process.

It was necessary to minimize the dispersion in the system. Once the dispersion compensating link was built and inserted into the system (see chapter A.3), the mirror and lens were adjusted together so the distance between them remained constant but the distance to the grating was modified slightly on each test. Cross-correlations were run until the pulse was at a minimum FWHM. Performing this part of the system alignment used the pulse shaper aparatus to minimize overall dispersion in the total system, which included both the pulse shaper apparatus and all fiber.

3.6.2 Insertion of Quarter Wave-plate and Single-layer LCM

Insertion of the QWP and single-layer LCM were very straight-forward. As depicted in figure 3.14, a polarizing beam splitter was inserted immediately after the collimator. The QWP was inserted with assistance of a translation stage. It was rotated until the power at (A) was maximized, which indicated that the optimal

birefringence angle was obtained because all available power passed through the polarizer, as discussed in section 2.3. Finally, the single-layer LCM was inserted between the lens and QWP in a manner similar to the procedure used for the two-layer LCM (refer to section 3.6.1).

4. POLARIZATION INDEPENDENT PULSE SHAPING

4.1 Compensation

Polarization insensitivity within in the system requires both phase-only operation and compensation of dispersion. The residual dispersion compensation is consistent for both the two-layer LCM and the combination of the quarter wave-plate and single-layer LCM. In sections 4.2 and 4.3, respectively, the methods behind compensation of higher-order terms will be discussed individually for the systems.

The spectral phase modulation caused by the dispersion in the fiber implies a frequency dependent refractive index $n(\omega)$. This does not change the pulse spectrum. To show this, begin with the expression for the phase term responsible for modulation of the positive portion of the electric field [5]:

$$\Psi(\omega) = -\frac{2\pi}{\lambda_0} n(\omega) d, \tag{4.1}$$

where d is the thickness of the optical medium, and λ_0 is the center wavelength. After passing through the fiber, the pulse suffers from chromatic dispersion and the different frequency components within the pulse have different paths because they are traveling with different time delays. This group velocity dispersion is reason to take the Fourier transform of the pulse, calculate the phase for each of the frequency components, and then perform the inverse Fourier transform to get the signal back to the time domain. Beginning with equation 4.1 and taking the Taylor series expansion of the phase term $\Psi(\omega)$ around the central frequency ω_0, the following is obtained:

$$\Psi(\omega) = \Psi(\omega_0) + \left|\frac{d\Psi(\omega)}{d\omega}\right|_{\omega_0} (\omega - \omega_0) + \left|\frac{1}{2}\frac{d^2\Psi(\omega)}{d\omega^2}\right|_{\omega_0} (\omega - \omega_0) + \cdots. \tag{4.2}$$

Simplifying equation 4.2 yields:

$$\Psi(\omega) = b_0 + b_1(\omega - \omega_0) + \frac{1}{2} b_2 (\omega - \omega_0)^2 + \cdots, \tag{4.3}$$

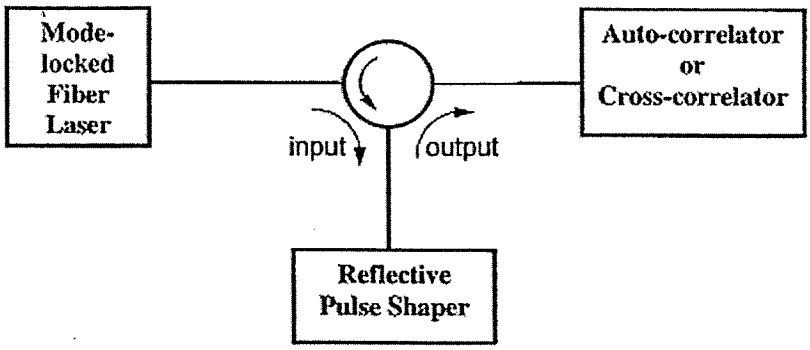

Fig. 4.1. Block diagram of entire system involved in the compensation implementation

where b_0 is a constant, b_1 gives the group delay and the linear spectral coefficient, b_2 gives the linear spectral chirp, and b_n gives the $(n-1)^{th}$ spectral chirp.

4.1.1 Residual Dispersion Compensation

The pulse shaper serves the purpose of taking the Fourier transform in a complete optical system. The pulse shaper input is a pulsed light source through a circulator, as described in section 3.4.2. Figure 4.1 shows a simplified schematic of the entire system including the pulsed light source and the measurement detector.

The laser source is an additive pulse mode-locked erbium fiber ring laser [27]. When it is mode-locked, the laser outputs nominally 70 fs pulses with a 60 nm FWHM centered at 1578 nm.

The SMF fiber in the system causes a broadening of the output pulses before the signal reaches the correlator used for temporal pulse measurement. This broadening is mostly compensated by the DCF fiber included in the output link, as described in chapter A.3. However, a small amount of dispersion is caused by the imperfect alignment of the pulse shaper. In the case of the pulse shaper used for this set of experiments, the pulse shaper compensates for the imperfections in the DCF

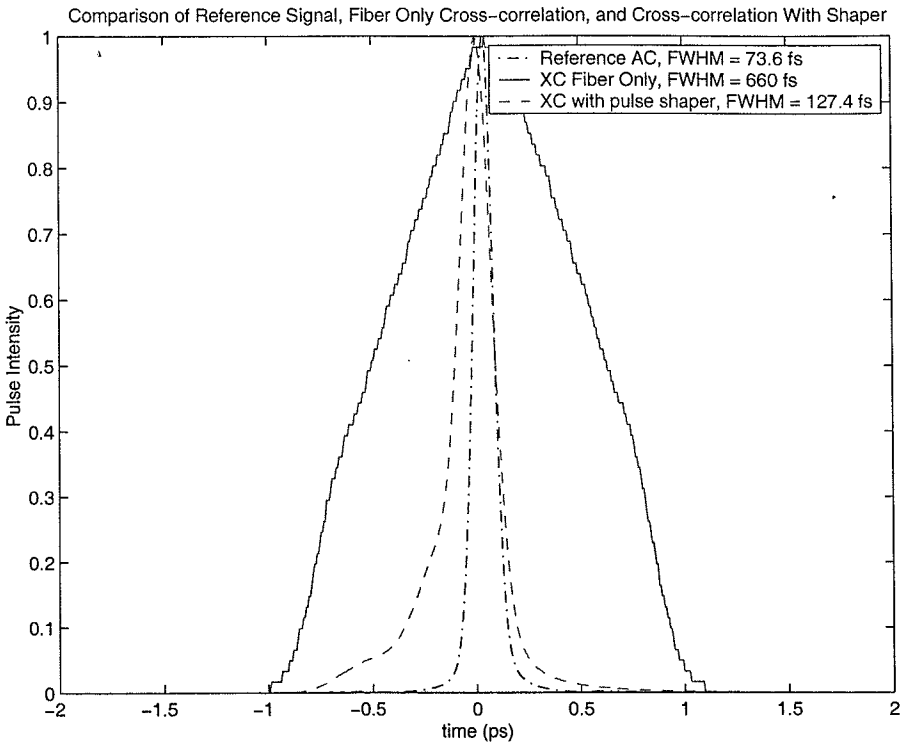

Fig. 4.2. The FWHM of the signal is broadened after passing through 39.8m of total fiber. The pulse shaper compensates some of the fiber to result in a temporally restored pulse.

compensation of the overall system SMF chromatic dispersion. Figure 4.2 shows the effect of the of the pulse shaper on the pulse FWHM. The pulse shape is unchanged by the pulse shaper. The pulse shaper is used solely to compensate for some of the chromatic dispersion in the fiber link. Also included in figure 4.2 is the original pulse when an auto-correlation is performed on the signal.

Figure 4.3 shows only the cross-correlation of the uncompensated pulse. There is uncompensated residual cubic dispersion, as indicated by the asymmetric ringing tail (refer back to table A.1). Note that the units on the vertical scale are in mV instead of an optical power unit such as mW because the optical power of the pulse shaper output signal is detected by a photomultiplier tube and the resulting signal is digitized.

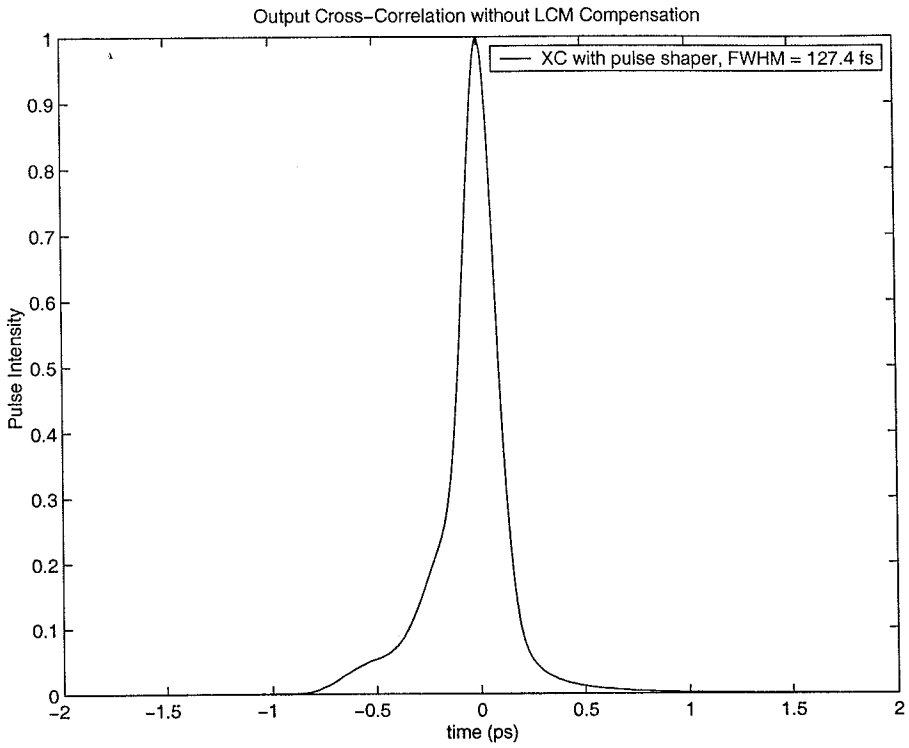

Fig. 4.3. Resultant cross-correlation after pulse shaper is put into place. The 'ringing' tail indicates the presence of cubic dispersion.

4.2 Two-layer Programmable Phase Masks

Since the mirror is located at the beam waist, the mask is moved slightly out of focus and operates on frequency spots that are not truly at their minimum. In the previous set of experiments, this effect was negligible because the mask was close to the mirror relative to the lens focal length. The same assumption was made in this set of experiments, which duplicate those efforts.

The calibration curves were first loaded into the computer and the LCM mask was activated. The computer program allows the user to successively test many masks quickly. The LCM was operated in common mode, which means that the same phase profile was applied to the two layers of the LCM. The optimum phase profile shown in figure 4.4 minimizes the pulse width. The cubic profile is composed

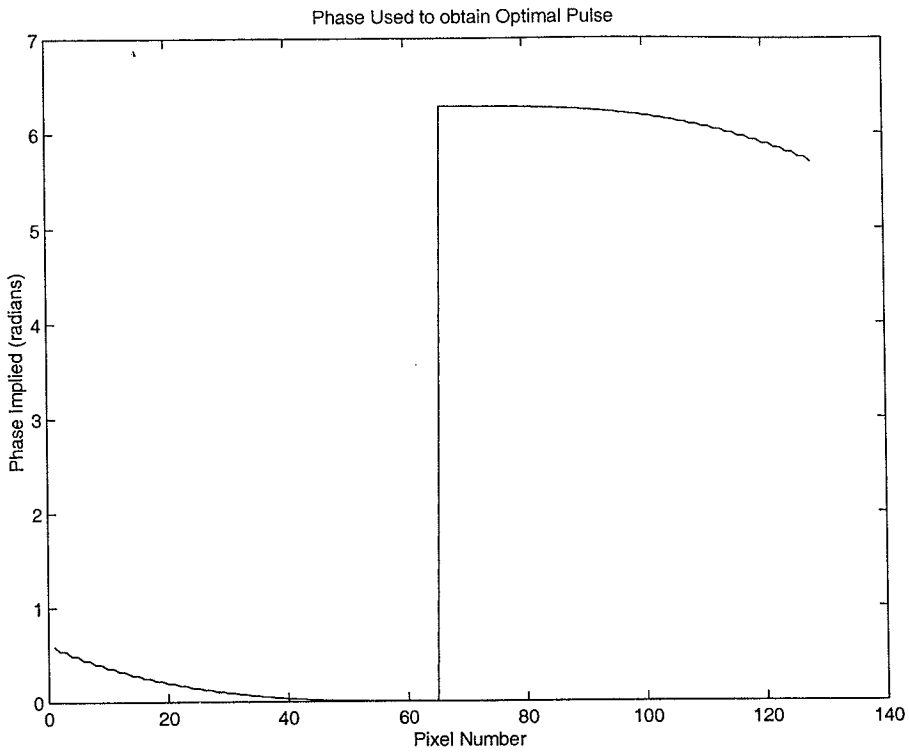

Fig. 4.4. Phase profile applied via LCm to obtain the optimal pulse out of the system.

of 128 discrete phase values with modulo 2π discontinuities. The optimum phase profile is shifted from the center of the peak of the spectrum to compensate for the quadratic phase dispersion that was still remaining in the system. The resultant intensity cross-correlation is also shown in figure 4.5.

The pulse shown is a symmetric pulse with a precipitate maximum and a FWHM $= 82.6fs$. This indicates that much of the quadratic and cubic phase is compensated with the LCM. The resultant pulse was not identical to the reference pulse, however, because some cubic phase was left uncompensated. The pulse width $\triangle t$ is able to be deconvolved using the deconvolution factor for a secant hyperbolic as indicated in table 3.1 and in equation 4.4. Equation 4.4 probably underestimates the pulse width

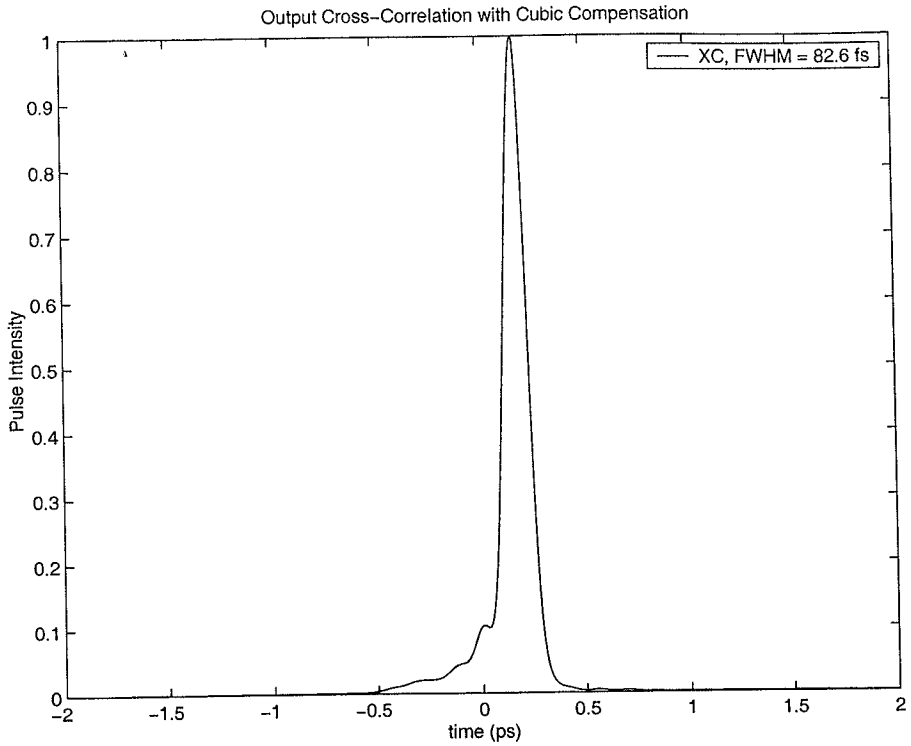

Fig. 4.5. Resultant intensity cross-correlation when the cubic phase is compensated via a phase-only control of the LCM.

because if the reference pulse is shorter than the signal pulses, the cross-correlation gives a reasonable direct estimate of the intensity profile.

$$\frac{FWHM}{1.55} = \triangle t. \tag{4.4}$$

The pulse relative to the zero time position is insignificant because it is set by the electronics relative to the starting location of the delay stage. Thus, only the shape of the pulse, as with the remaining sections in this chapter, is important. In the previous set of experiments, shaped pulses were next created. The waveforms were a superposition of the phase compensation mask and another pulse shape spectral phase mask. The previous set of experiments were confirmed to be polarization-independent and details are described in the previous work so the results have not been repeated here [4].

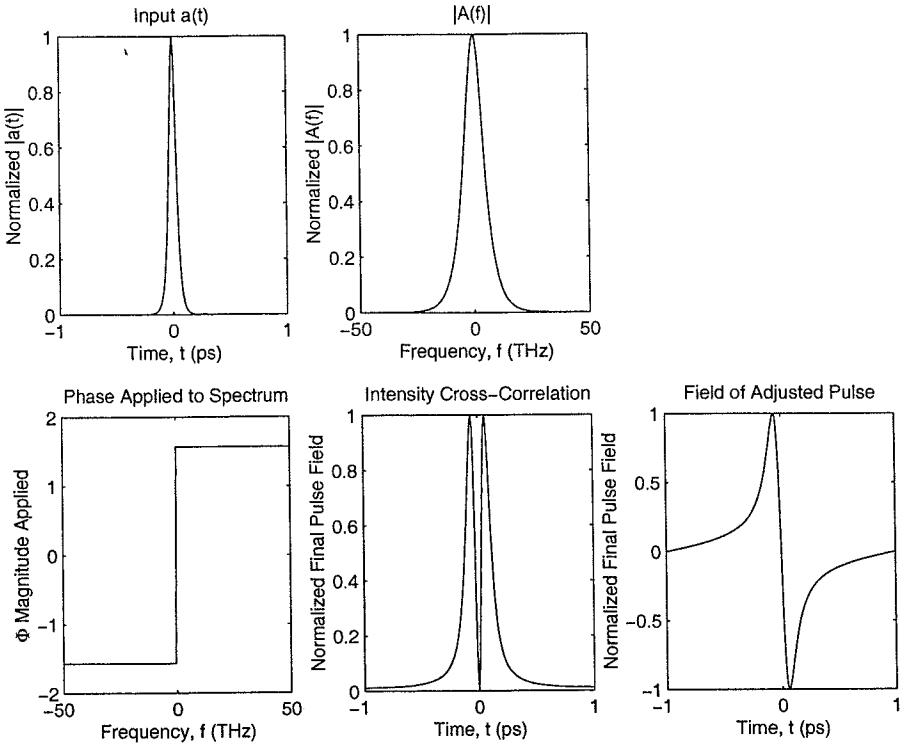

Fig. 4.6. Matlab simulation of the pulse obtained when a π phase is imposed on half of the spectrum by the LCM.

To demonstrate pulse shaping abilities with the two-layer system, an odd pulse was created by implying a π phase shift on half of the spectrum. Figure 4.6 shows a simulation of the system, displaying that the expected frequency domain mask results in a time domain pulse with a broader temporal FWHM and two peaks in the intensity cross-correlation instead of the single peak put into the system.

Since the pulse shaper operates using a reflection geometry, the signal is affected by the LCM phase mask twice so half of the desired phase shift, or a phase shift of $\frac{\pi}{2}$ is implied on the LCM mask. Figure 4.7 shows the mask pattern used in the system to produce the odd pulse and the resultant cross-correlation of the signal with the reference from the laser.

There are differences between the simulation and the results that must be noted. The simulation was created using many more resolution units than exist in the actual

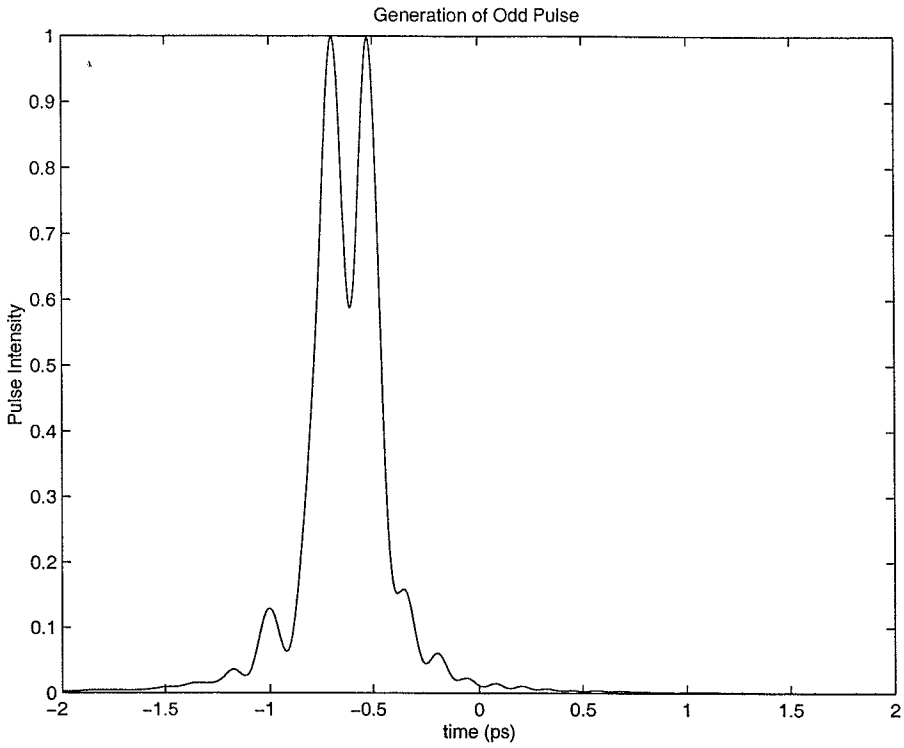

Fig. 4.7. Intensity cross-correlation when an odd pulse is generated by using the LCM to imply a π phase on half of the spectrum.

experiment. Thus, the output in the simulation is a smooth pulse. However, in the actual results, the output has few resolution units and a loss of resolution is observed immediately. The actual results also contain some ringing in the tail.

4.3 Single-layer Programmable Phase Masks

As mentioned in section 4.1, the extraordinary axes of the two layers in the two-layer LCM are offset by a total phase of 90^o. Thus, the two-layer LCM is replaced by a single-layer LCM and a quarter wave-plate. The LCM operates on vertically polarized light so when the signal first reaches it in the pulse shaper, the phase mask applied on the single-layer LCM without a polarizer acts on the vertically polarized signal component. The signal then passes through the quarter wave-plate and the

polarization is changed by $\frac{\lambda}{4}$. It then reflects off the gold mirror and passes through the quarter wave-plate where another $\frac{\lambda}{4}$ shift is implied. Since the LCM was used previously to take the Fourier transform of the signal, it is in the spectral domain and the two implied phase shifts add, producing the desired change in the polarization by $\frac{\lambda}{2}$. When the light passes through the LCM again, it has been shifted by a 90^o angle and it operates on the current horizontally polarized light components which were the unaffected vertical light components upon inital pass of the LCM. Thus, the single-layer LCM/QWP combination acts as a single-pass reflective pulse shaper as opposed to the two-pass system of the 2-layer LCM system. The mathematics behind this heuristic argument shall be explained in section 4.3.1. They are followed by a discussion of the loss of resolution in the shaper as a result of moving the LCM further from the gaussian beam waist in section 4.3.2, which is necessary to have the phase implied on the signal by the quarter wave-plate add as in the heuristic argument of the single-layer pulse shaper apparatus.

4.3.1 Mathematics

A schematic of the design of the quarter wave-plate and the single-layer LCM is shown in figure 4.8 in addition to a simplified view of the effective optics when the system is unfolded across the reflective mirror boundary.

In the spectral domain, the phase of each of the two wave-plates can be added to obtain an effective phase of the wave-plates. Thus, the QWP has an effective phase of 90^o, as shown in figure 4.9. The Jones matrix for each of the three components

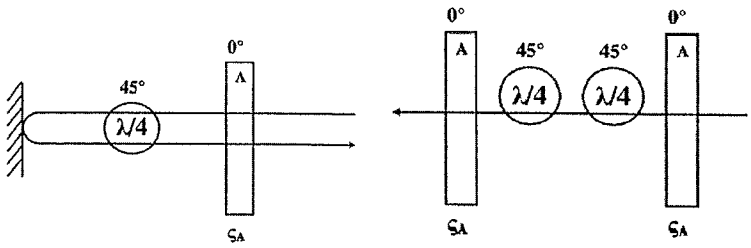

(a) Basic schematic of the single-layer LCM and QWP design.

(b) Unfolded schematic of the single-layer LCM and QWP design showing the component symmetry.

Fig. 4.8. The reflective design of the QWP and single-layer LCM are shown in their basic schematic format and also in the 'unfolded' layout to show component symmetry.

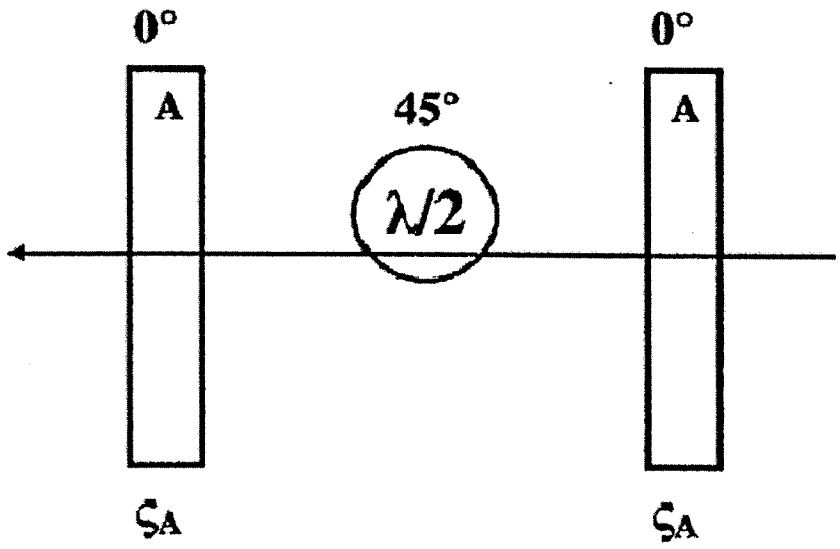

Fig. 4.9. The two QWPs are shown as the equivalent HWP.

can be combined to form the overall effective matrix on the system:

$$\begin{bmatrix} e^{-j\zeta_{LCM_x}} & 0 \\ 0 & e^{-j\zeta_{LCM_y}} \end{bmatrix} \begin{bmatrix} 0 & j \\ j & 0 \end{bmatrix} \begin{bmatrix} e^{-j\zeta_{LCM_x}} & 0 \\ 0 & e^{-j\zeta_{LCM_y}} \end{bmatrix} =$$

$$\begin{bmatrix} e^{-j\zeta_{LCM_x}} & 0 \\ 0 & e^{-j\zeta_{LCM_y}} \end{bmatrix} \begin{bmatrix} 0 & je^{-j\zeta_{LCM_y}} \\ je^{-j\zeta_{LCM_x}} & 0 \end{bmatrix} = \tag{4.5}$$

$$\begin{bmatrix} 0 & je^{-j\left(\zeta_{LCM_x}+\zeta_{LCM_y}\right)} \\ je^{-j\left(\zeta_{LCM_x}+\zeta_{LCM_y}\right)} & 0 \end{bmatrix} =$$

$$je^{-j\left(\zeta_{LCM_x}+\zeta_{LCM_y}\right)} \begin{bmatrix} 0 & 1 \\ 1 & 0 \end{bmatrix}$$

where $\zeta_{LCM_x} = \omega n_{ORDINARY} \frac{L_{LCM}}{c}$ and , $\zeta_{LCM_y} = \omega n_{EXTRAORDINARY} \frac{L_{LCM}}{c}$.

The output signal is dependent on a phase of $je^{-j\left(\zeta_{LCM_x}+\zeta_{LCM_y}\right)}$ acquired by the field, as shown in the final term of equation 4.5. The matrix expression in the final result transforms the polarization state. This means that when the extraordinary and ordinary axes of the QWP are aligned at angles of $\pm 45^o$, as previously assumed, the polarization transformation is independent of the phase applied. Stated more simply, the HWP of figure 4.9 performs the operation of swapping the $x-$ and $y-$components of the signal polarization state but otherwise maintains polarization-independent pulse shaping.

4.3.2 Loss of Resolution

The beam diameter incident on the LCM is larger than the beam diameter at the beam waist in both the two-layer and single-layer systems. This effect is amplified as the LCM gets further from the focal plane and the mirror, resulting in degradation of resolution, and must be considered for the single-layer system because of the

requirement that the quarter wave-plate be placed between the LCM and the mirror in the pulse shaping apparatus. The relationship is defined by [24]:

$$w^2(z) = w_f^2 \left[1 + \left(\frac{z}{z_f} \right)^2 \right] \tag{4.6}$$

where w_f is the beam radius at the focal plane, defined by:

$$w_f = \frac{f\lambda}{\pi w_b}. \tag{4.7}$$

and

$$w_b = \frac{w_i cos\theta_d}{cos\theta_i}, \tag{4.8}$$

as defined previously in chapter ??. In equations 4.6 and 4.7, w_b is the diffracted beam radius, z is the distance of the beam along the plane in which it is traveling, n is the refractive index of the propagation media, $z_f = \frac{\pi w_f^2}{\lambda}$ is the distance from the beam waist at which the beam has spread by a factor of $\sqrt{2}$, and λ is the optical wavelength.

It is also important to note that [25]:

$$b = \frac{2\pi}{\lambda} w_f^2 = 2z_f, \tag{4.9}$$

where w_f is still the beam radius at the focal plane, λ is the optical wavelength, and b is the Gaussian beam focal depth (also called the confocal parameter).

Physically, $\frac{b}{2}$ is the distance between two planes in which the beam radius changes from w_0 to $\sqrt{2}w$. If $\frac{b}{2} \gg L_{aperture}$, where $L_{aperture}$ is the distance from the beam waist to the LCM pixel location, the beam diffraction effect does not need to be included in the system calculations for resolution.

Inspecting equations 4.6 and 4.9 makes the effect of moving the LCM further from the focal plane very clear. For the single-layer pulse shaper used in this set of experiments, the expected resolution of $2w(z)$ was 560 μm, or 6 pixels. The parameters required to determine the expected resolution are given in table 4.1.

Table 4.1: Values of the parameters given by equations 4.6, 4.7, 4.8, and 4.9, which were used to determine the expected resolution in the single-layer system and also in the single-layer system if a special QWP holder were designed and built that would add no additional thickness to the QWP but still maintain precise rotational alignment. The grating parameters dicussed in chapter ?? are also repeated.

Parameter	**Symbol**	**1-layer System**	**Special Holder**
Grating incident beam radius	w_i	$\frac{1.9}{2}$ mm	$\frac{1.9}{2}$ mm
Beam diffraction angle	θ_d	53^o	53^o
Grating incident angle	θ_i	70^o	70^o
Diffracted beam radius	w_b	1.7 mm	1.7 mm
Laser center wavelength	λ	1578 nm	1578 nm
Lens focal length	f	145 mm	145 mm
Beam radius at the focal plane	w_f	43.6 μm	43.6 μm
Confocal parameter	b	7.6 mm	7.6 mm
Distance at which the beam has spread from w_0 to $\sqrt{2}w$	z_f	3.8 mm	3.8 mm
Distance from beam waist to LCM incidence plane	z	24 mm	12 mm
Beam radius at the LCM incidence plane	$w(z)$	280.1 μm	145.5 μm

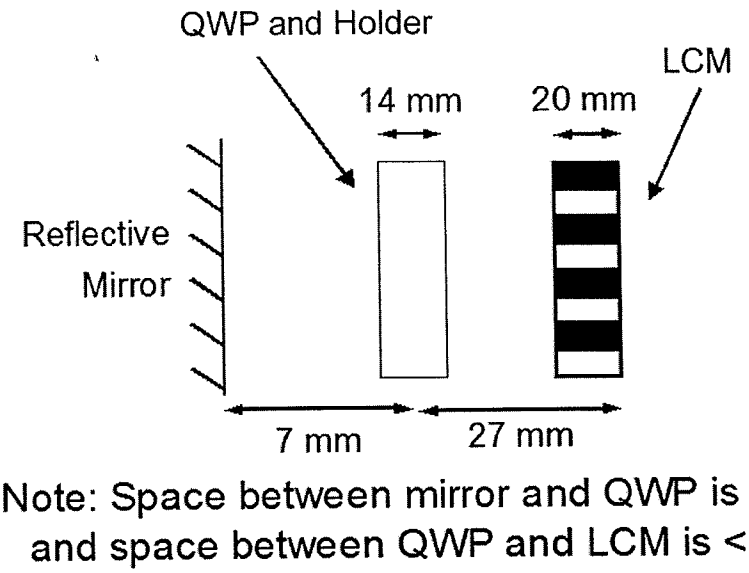

Fig. 4.10. Basic layout of the system near the mirror showing the distance from the mirror through the QWP and the single-layer LCM.

On the single-layer setup, the LCM layer is 20 mm thick so the assumption is made that $L_{LCM} = 10$ mm, $L_{QWP} = 14$ mm including the thickness of the holder, and $L = L_{LCM} + L_{QWP} = 24$ mm, where L_{LCM} is the distance of the liquid crystal layer from the outer edge of the LCM closest to the reflective mirror and L_{QWP} is the distance from the outer edge of the LCM closest to the reflective mirror to the reflective mirror required for placement of the QWP, as indicated by figure 4.10. The measured resolution for this setup is 400μm, corresponding to 4 LCM pixels, which was obtained experimentally by turning on one pixel of the LCM at a time and observing the peak spectral amplitude out of the setup on an OSA. The effective resolution is determined at the point where turning on more LCM pixels does not increase the peak spectral amplitude, but only broadens the observed spectral width [25].

If one were to design and build a special QWP holder that would add no additional thickness to the QWP but still maintain precise rotational alignment, this set of calculations may be repeated to determine that the resolution could be improved.

In order to obtain an estimate of the potential resolution enhancement, assume that a QWP and holder assembly could be fabricated such that the total thickness was on the order of 2 mm. This would imply a total distance from the focal plane to the LCM aperature, $L_{aperture}$, of 12 mm. Inserting this value into equation 4.6 results in a beam radius of 145 μm at the LCM implying an effective resolution equal to $2w(z)$ of 290 μm or 3 pixels.

Optimization is possible on the resolution on the system through varying the parameters defined in table 4.1. For example, one could desire the best possible resolution while maintaining all components aligned as they were but only modifying the radius of the colimated beam incident on the grating. The following procedure would be used to determine the optimal resolution and grating beam diameter required. First, equation 4.9 would be solved for z_f. This would then be inserted into equation 4.6. The result would then be differentiated with respect to w_f and solved for the zeros. The zeros of the equation are the w_f values that minimize w. Then, using the known f, λ, and θ_i, θ_d, and equations 4.7 and 4.8, the corresponding colimated beam radius, w_i, can be found.

For the single-layer system, the total distance from the focal plane to the LCM aperature, $L_{aperture}$, is 24 mm, and calculated minimum beam radius calculated would be 155.3 μm at the LCM implying an effective resolution equal to $2w(z)$ of 310 μm or just over 3 pixels when a colimated beam of radius of 1.2 mm (2.4 mm diameter) is used. For the case in which a special QWP holder were to be designed and built, the total distance from the focal plane to the LCM aperature, $L_{aperture}$, is 12 mm, and calculated minimum beam radius calculated would be 109.8 μm at the LCM implying an effective resolution equal to $2w(z)$ of 220 μm or just over 2 pixels when a colimated beam of radius of 0.6 mm (1.2 mm diameter)is used.

4.3.3 Odd Pulse

Refer to figure 4.6 for a simulation of the odd pulse generation within the system by application of a π phase shift on half of the spectrum.

Figure 4.11 shows the mask pattern used in the system to produce the odd pulse and the resultant cross-correlation of the signal with the reference from the laser. These results were obtained using an uncompensated pulse to show that odd pulse generation was possible.

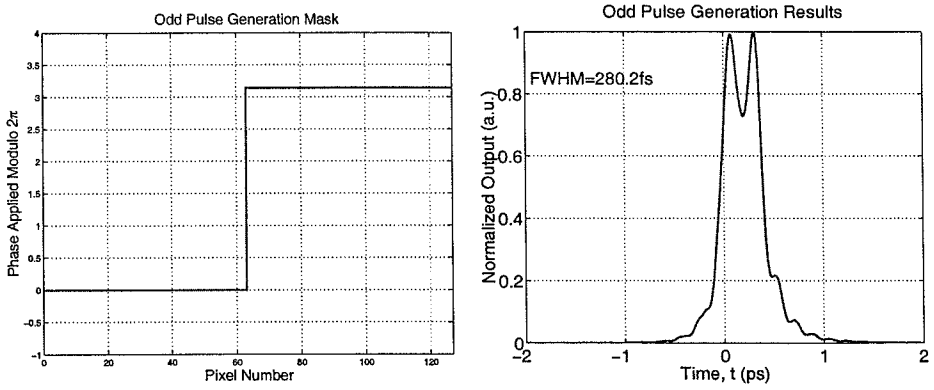

(a) Odd Pulse Generation Mask (b) Odd Pulse Generation Results

Fig. 4.11. The phase mask and resultant intensity cross-correlation when an odd pulse is generated by using the single-layer LCM to imply a π phase on half of the spectrum.

4.3.4 Polarization Insensitivity Demonstration

The fiber ring laser used for this set of experiments is home-built and has some variation in the output. Thus, it was important to take cross-correlation measurements and optimize the pulse prior to each use. Figure 4.12 shows the initial cross-correlation results when the doublet and cubic pulses were generated.

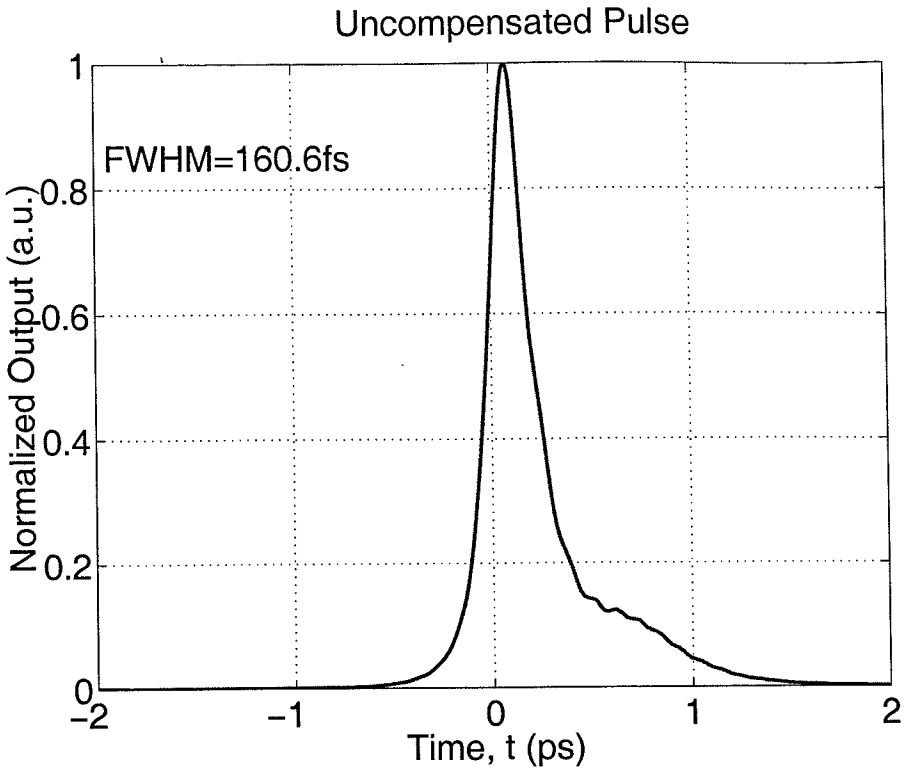

Fig. 4.12. Intensity cross-correlation prior to spectral phase compensation. The single-layer LCM and QWP were in place but no phase was implied to the spectrum by the LCM.

To demonstrate that the pulse shaper is polarization insensitive, the polarization controller was used to send several polarization input states to the pulse shaper and the output was compared. Six different polarization states were selected arbitrarily for each of the pulse shapes investigated. The states were consistent for all of the pulse shapes listed under a given polarization state. Each of the polarization states are shown on the polarization sphere in figure 4.13.

Note that the cross-correlator is maximized when the input polarization to the cross-correlation setup is nearly horizontal so a second polarization was controller placed immediately before the correlator setup to account for this requirement.

As indicated by figure 4.15, the input polarizations do not affect the compensated pulse significantly. This is also demonstrated by inspecting figures 4.14, 4.17, and

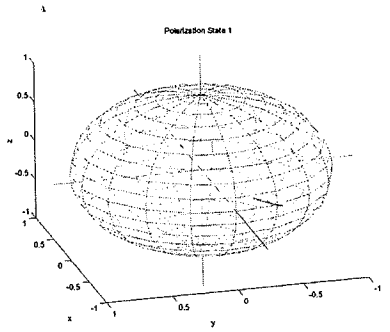

(a) Polarization State 1

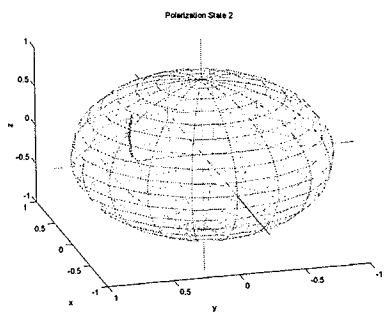

(b) Polarization State 2

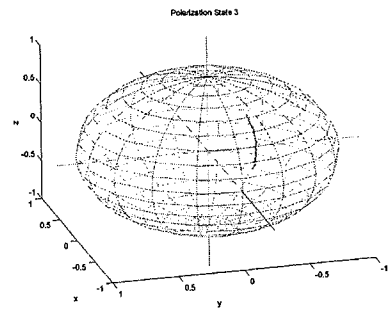

(c) Polarization State 3

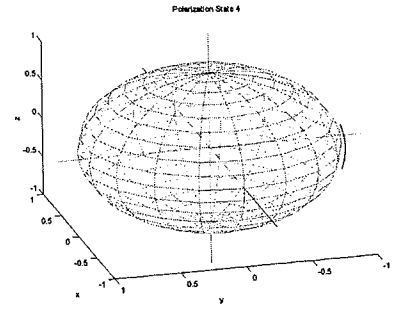

(d) Polarization State 4

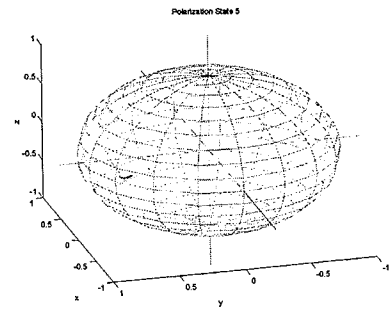

(e) Polarization State 5

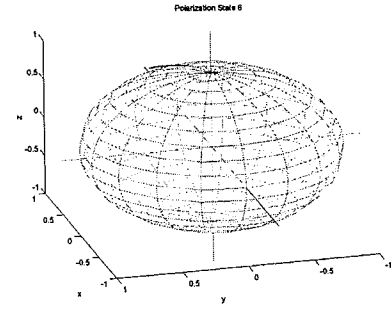

(f) Polarization State 6

Fig. 4.13. The polarization states used to demonstrate polarization-insensitivity are shown on the polarization sphere. A wavelength-dependent polarimeter [28] was used to obtain the polarization states on the sphere. It was not calibrated prior to use because only the relative positions of the polarization states were desired.

4.18, which result from the generation of the odd pulse, the doublet and opposite cubic pulses, respectively. Figure 4.16 shows the phase profiles used to obtain the two cubics.

Figure 4.15 shows the polarization insensitivity of the optimal pulse obtained through spectral phase compensation prior to application of the additional phase masks used to generate each of the pulse shapes.

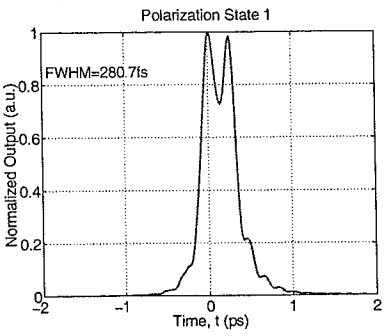

(a) Polarization State 1

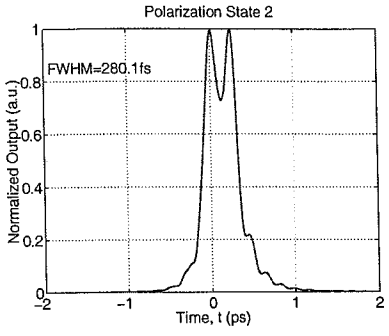

(b) Polarization State 2

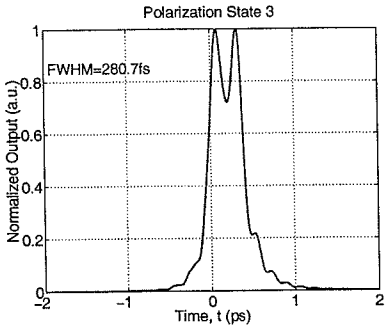

(c) Polarization State 3

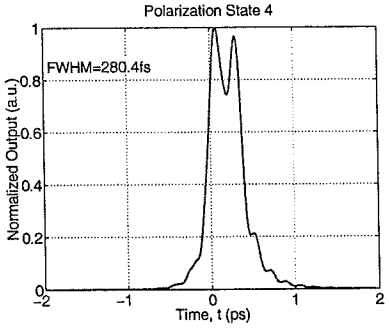

(d) Polarization State 4

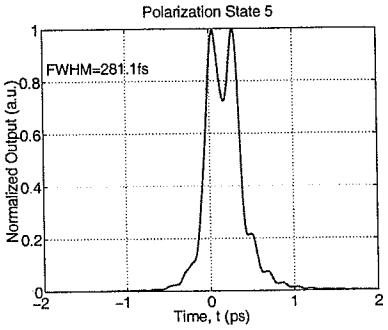

(e) Polarization State 5

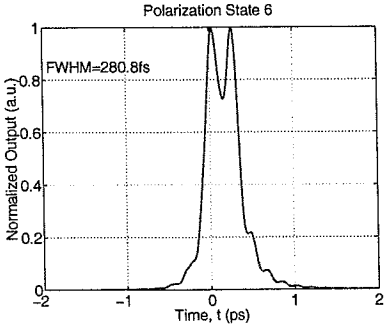

(f) Polarization State 6

Fig. 4.14. Dispersion compensated odd pulses with deconvolved pulse width $\triangle t$ and peak signal level shown to demonstrate polarization independence. These pulses were produced using an uncompensated pulse to confirm proper calibration and appropriate LCM control.

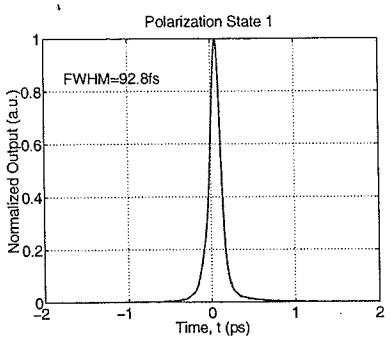

(a) Polarization State 1

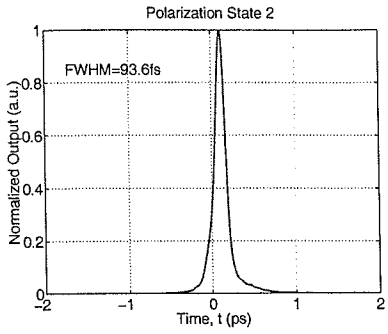

(b) Polarization State 2

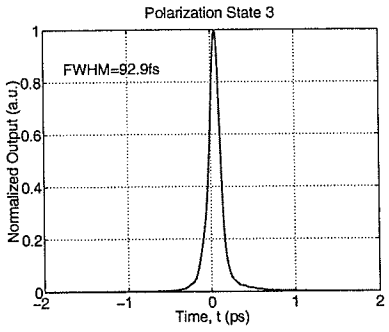

(c) Polarization State 3

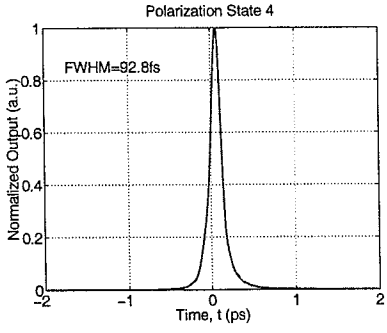

(d) Polarization State 4

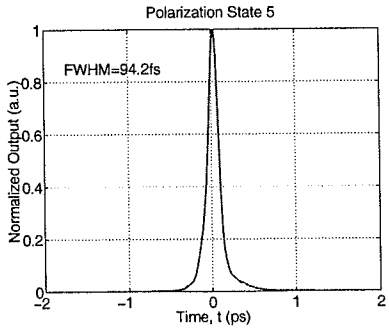

(e) Polarization State 5

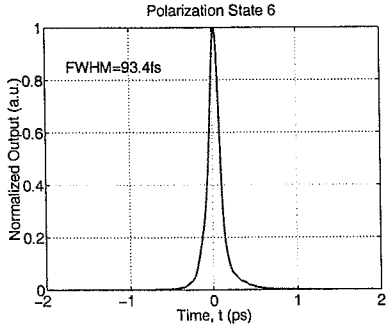

(f) Polarization State 6

Fig. 4.15. Intensity cross-correlation after spectral phase compensation. The phase mask used to obtain the optimum pulse was maintained in addition to the phase masks used to generate the doublet and the cubic pulses.

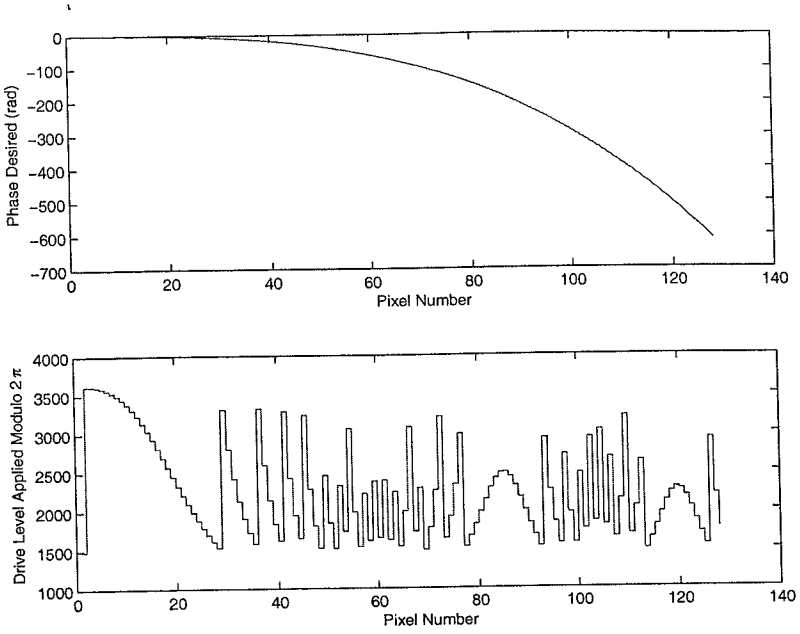

(a) Phase mask used to generate cubic shown in figure 4.17.

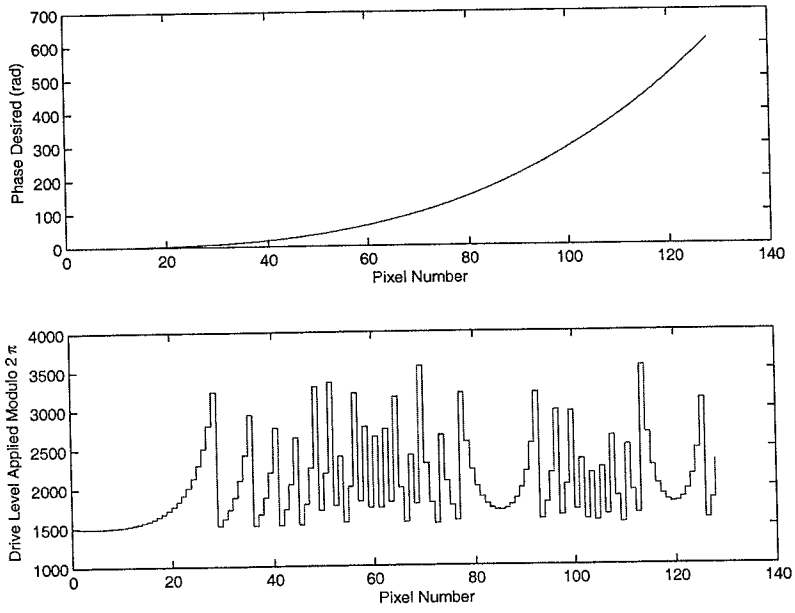

(b) Phase mask used to generate cubic shown in figure 4.18.

Fig. 4.16. Phase profiles used to generate cubic pulses

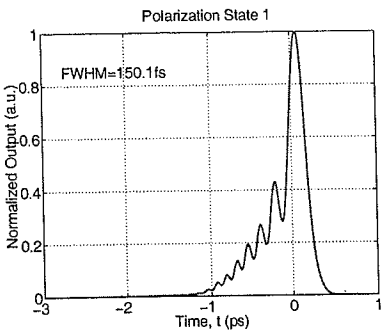

(a) Polarization State 1

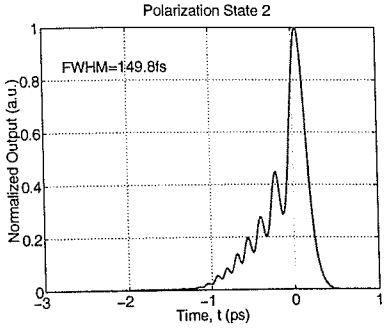

(b) Polarization State 2

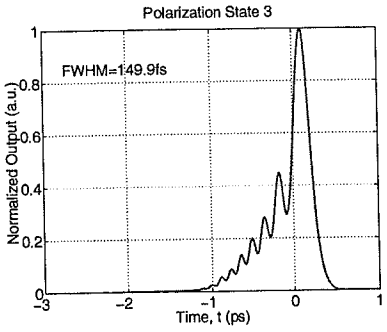

(c) Polarization State 3

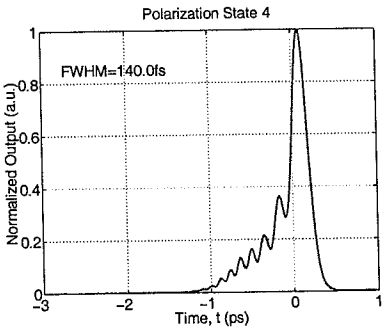

(d) Polarization State 4

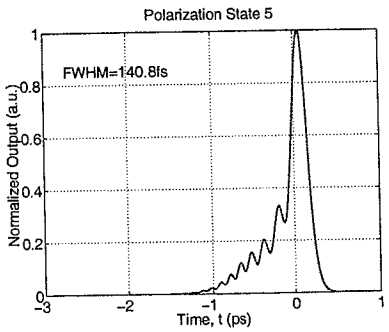

(e) Polarization State 5

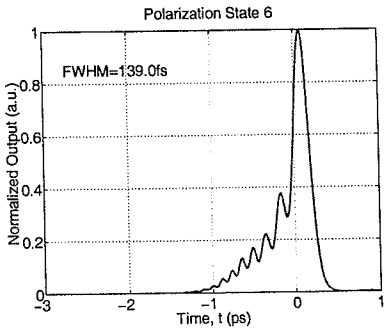

(f) Polarization State 6

Fig. 4.17. Dispersion compensated cubic pulses with deconvolved pulse width $\triangle t$ and peak signal level shown to demonstrate polarization independence.

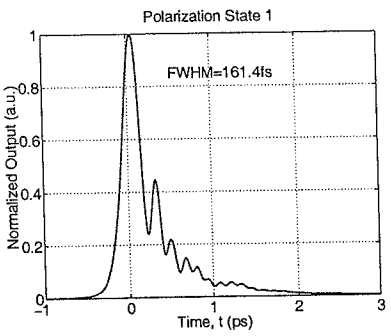

(a) Polarization State 1

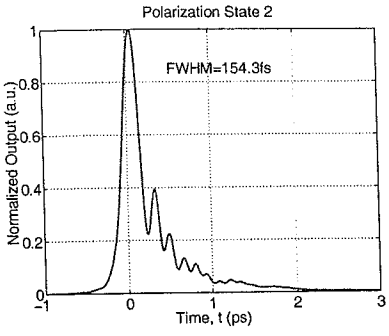

(b) Polarization State 2

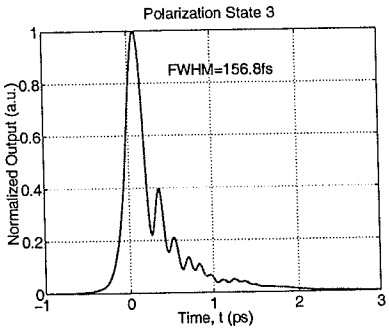

(c) Polarization State 3

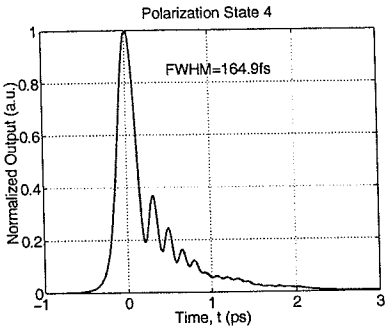

(d) Polarization State 4

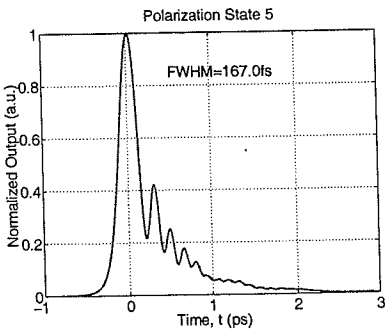

(e) Polarization State 5

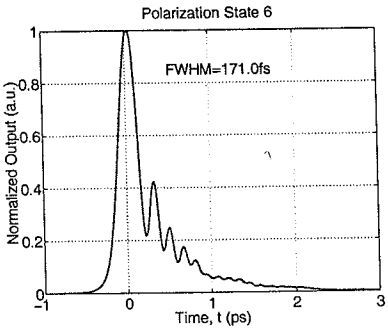

(f) Polarization State 6

Fig. 4.18. Dispersion compensated cubic pulses with deconvolved pulse width $\triangle t$ and peak signal level shown to demonstrate polarization independence.

5. SUMMARY AND CONCLUSIONS

A previous system demonstrated the ability to be used as a programmable polarization independent pulse compensator with low loss. The apparatus operated through a costly two-layer modulator technology. The focus of this project was to demonstrate that the goals of the previous system could be accomplished with a more economical alternative, while still maintaining the requirements of fine-tunability, polarization independence, and high efficiency.

LIST OF REFERENCES

[1] H.J.R. Dutton. *Understanding Optical Communications.* IBM's International Technical Support Organization, 1998. www.redbooks.ibm.com.

[2] R. Ramaswami and K.N. Sirvarajan. *Optical Networks: A Practical Perspective.* Morgan Kaufmann Publishers, San Francisco, 1998.

[3] G.P. Agarwal. *Nonlinear Fiber Optics.* Academic Press, San Diego, 2001. p. 98.

[4] R.D. Nelson. Programmable polarization independent spectral phase compensation and shaping of femtosecond optical pulses. Master's thesis, School or Electrical and Computer Engineering, Purdue University, May 2003.

[5] E. Hecht. *Optics.* Addison Wesley Longman, Reading, MA, second edition edition, 1998.

[6] S. Ramo, J.R. Whinnery, and T. Van Duzer. *Fields and Waves in Communication Electronics.* John Wiley and Sons, New York, 1993. pp. 280-283.

[7] M. Akbulut. Computer modeling for characterization, emulation and compensation of polarization mode dispersion in single-mode fibers. Master's thesis, School or Electrical and Computer Engineering, Purdue University, May 2001.

[8] Sophocles J. Orfanidis. *Electromagnetic Waves and Antennas*, chapter Uniform Plane Waves. http://www.ece.rutgers.edu/ orfanidi/ewa/ch02.pdf, June 2004.

[9] C.L. Chen. *Elements of Optoelectronics and Fiber Optics.* Irwin, Chicago, 1996. pp. 309-331.

[10] D.S. Kliger, J.W. Lewis, and C.E. Randall. *Polarized Light in Optics and Spectroscopy.* Academic Press, Boston, 1990.

[11] E.W. Weisstein. World of physics: Jones vector. http://www.scienceworld.wolfram.com/physics/JonesVector.html, 2004. Optics, Online.

[12] Melles griot: Quarter wave-plate. http://www.mellesgriot.com. Optics, Online.

[13] C. Rulliere. Femtosecond laser pulses. principles and experiments. Technical report, Springer, 1998.

[14] A.M. Weiner. Ultrafast optics class notes. West Lafayette, IN: Purdue University, 2004.

[15] A.M. Weiner. Femtosecond pulse shaping using spatial light modulators. *Review of Scientific Instruments*, 71(5):1929–1960, May 2000.

[16] A.M. Weiner et al. Programmable femtosecond pulse shaping by use of a multielement liquid-crystal phase modulator. *Optics Letters*, 15(6):326–328, Mar. 1990.

[17] A.M. Weiner et al. Programmable shaping of femtosecond optical pulses by use of 128-element liquid crystal phase modulator. *IEEE Journal of Quantum Electronics*, 28(4):908–920, Apr. 1992.

[18] M.M. Wefers and K.A. Nelson. Generation of high-fidelity programmable ultrafast optical waveforms. *Optics Letters*, 20(9):1047–1049, May 1995.

[19] C.-C. Chang, H.P. Sardesai, and A.M. Weiner. Dispersion-free fiber transmission for femtosecond pulses by use of a dispersion-compensating fiber and a programmable pulse shaper. *Optics Letters*, 23(4):283–285, Feb. 1998.

[20] S. Shen and A.M. Weiner. Complete dispersion compensation for 400-fs pulse transmission over 10-km fiber link using dispersion compensating fiber and spectral phase equalizer. *IEEE Photonics Technology Letters*, 11(7):827–829, July 1999.

[21] H. Wang et al. 20-fs pulse shaping with a 512-element phase-only liquid crystal modulator. *IEEE Journal on Selected Topics in Quantum Electronics*, 7(4):718–727, Jul./Aug. 2001.

[22] Cambridge Research and Instrumentation, Inc. (CRI). *Spatial Light Modulator System*, 2003.

[23] C. Palmer. *Diffraction Gratings Handbook.* Spectra-Physics, Rochester, NY, 2002.

[24] J.T. Verdeyen. *Laser Electronics.* Prentice Hall, Upper Saddle River, NJ, 1995. pp. 63-85.

[25] Z. Jiang. Reflective pulse shaper design with high resolution / low loss. Ultrafast Optics and Optical Fiber Communications Laboratory at Purdue University, Jan. 2004.

[26] P.F. McManamon et al. Optical phased array technology. *Proceedings of the IEEE*, 84(2):268–298, Feb. 1996.

[27] K. Tamura, H.A. Haus, and E.P. Ippen. Self-starting additive pulse mode-locked erbium fibre ring laser. *Electronics Letters*, 28(24):2226–2228, Nov. 1992.

[28] S.X. Wang and A.M. Weiner. Fast wavelength-parallel polarimeter for broadband optical networks. *Optics Letters*, 29:923–925, May 2004.

APPENDICES

APPENDIX A
DISPERSION COMPENSATION

Dispersion causes separation of a wave into its many wavelength components. There is strong dispersion in the fiber leads to the pulse shaper apparatus, which must be compensated so that the effect of the pulse shaper can be observed. Thus, it is a critical portion of the overall system and must be addressed before the pulse shaper can be used to compensate for spectral phase. Common types of dispersion are given in table A.1. Second order dispersion, particularly chromatic dispersion, is the topic of this chapter as it arises from the refraction of the optical pulse within optical fiber.

Figure A.1 shows a basic layout of the pulse shaping apparatus. At this point, it is important to note that the pulse is in fiber until it passes through the collimator to free space. After reflecting off the mirror, it remains in free space until it enters the collimator again, at which point it is again in fiber. It remains in fiber thereafter.

The process of compensating chromatic dispersion is typically straightforward. However, if the dispersion compensating fiber is inconsistent, problems will arise. The problems that arose in the process of this work are first discussed followed by the solution and resultant compensation correlations.

In order for a useful cross-correlation measurement to be taken, both the timing and dispersion of the system must be correct. The timing will be discussed first followed by the dispersion compensation.

Table A.1
Common dispersion types and the corresponding electric field intensity profiles.

Order	Expression	Intensity Correlation
Quadratic ("Slope")	$\phi \propto \omega^2$	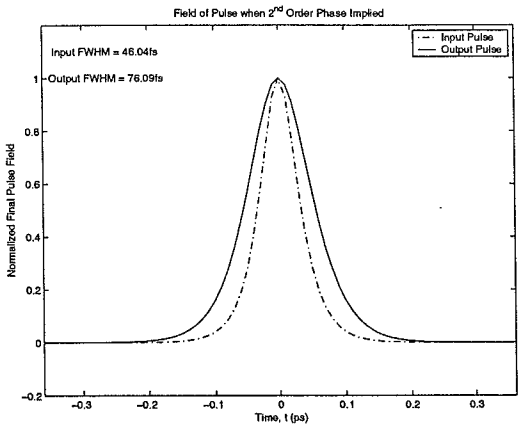
Cubic ("Chirp")	$\phi \propto \omega^3$	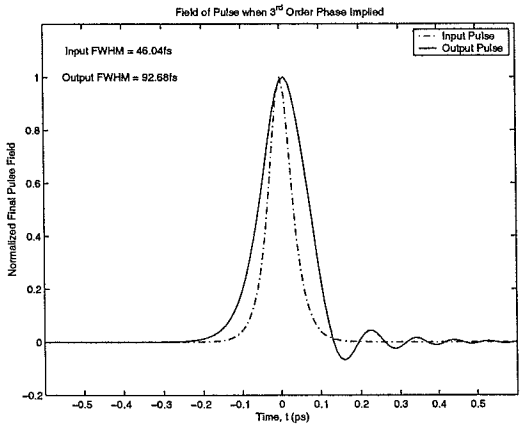

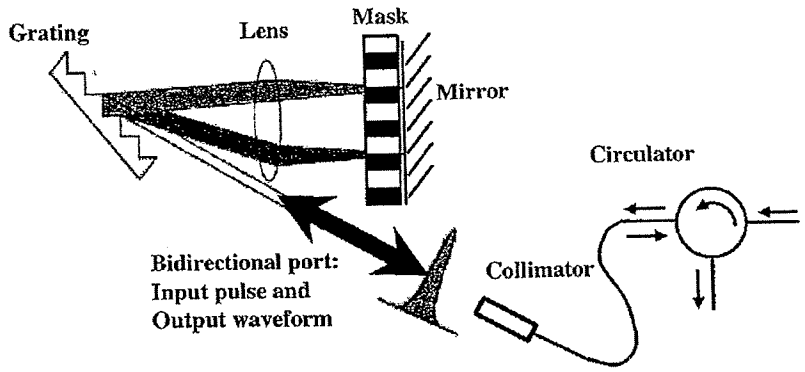

Fig. A.1. The pulse shaping apparatus is a combination of free space and fiber transmission. Chromatic dispersion occurs in the fiber portions of the overall system, which includes the measurement fibers in addition to the pulse shaper fiber.

A.1 Timing Calculation of Needed Fiber

The timing is correct when the signal used for reference overlaps the signal out of the entire system. This is found easily via simple experiment. The output from the shaper is put into a photodiode that converts the optical signal to an electric signal. A reference electric signal is obtained from a photodiode connected to the laser output. The reference electric signal is the time base for sampling on an oscilloscope. After viewing the temporal difference in the peaks of the two signals, a guess is made for the amount of fiber needed to delay the peak of the output signal so it matches the maximum on the reference signal. Inserting 104.2 cm of SMF to the signal path gave 5.14×10^{-9} s more delay to the signal. This was used to calculate the added delay needed to obtain the desired timing results. The total timing delay needed was 16.5 ns when the total output fiber length was 1135.6 cm. The long output fiber length

was required because of the physical layout of the laboratory and the measurement equipment.

$$\begin{gathered}\text{(Delay needed)}\left(\frac{\text{Added fiber}}{\text{Additional Delay}}\right) = \\ (16.5\text{ ns})\left(\frac{104.2\text{ cm}}{5.14ns}\right) = \\ 334.5\text{ cm more fiber needed.}\end{gathered} \tag{A.1}$$

This indicated that the total fiber needed to obtain the necessary overlap of the signal and the output pulse was 1135.6 cm + 334.5 cm = 1470.1 cm. This number was obtained with the polarization controller located after the circulator so the fiber was double-passed. Later, the polarization controller was moved so that it was placed prior to the circulator input and it became just single-passed. As a result, the length of the fiber in the polarization controller, 386.7 cm, was removed from the output link. This required that the total fiber needed to obtain delay had to account for the loss of fiber, which inevitably led to a change in the delay of the system and affected the overlap of the signal reference and the system output. The removal of the fiber had to be compensated by adding the length removed to the estimate of the total fiber link length needed to obtain appropriate timing considerations. Thus, 386.7 cm was added to the fiber length estimate required for a total fiber link length of T = 1856.8 cm needed. Before compensating for chromatic dispersion, the necessary fiber was added to the link to confirm the timing estimate was correct.

A.2 Dispersion Minimization

The amount of DCF inserted into a system has to compensate the entire amount of SMF in the system, including the output from the laser and the inputs to the measurement system. The lengths of all fiber involved are listed in tables A.2 and A.3, which list the fiber in the pulse shaper apparatus and the fiber in the overall system, respectively.

Table A.2

SMF lengths of all components in the pulse shaper that must be compensated for chromatic dispersion by DCF.

Mathematical Symbol	**Component**	**SMF Length**
PC	Polarization Controller	386.7 cm
$Circ_{1\rightarrow 2}$	$\text{Circulator}_{1\rightarrow 2}$	256.5 cm
Col	Collimator	235.5 cm
$Circ_{2\rightarrow 3}$	$\text{Circulator}_{2\rightarrow 3}$	266.3 cm

Since the pulse shaper is a reflective system, the optical signal passes through the collimator fiber twice. It was accounted for in the calculation of the total fiber length in the pulse shaper.

$$\begin{aligned} &\text{Total Pulse Shaper Length} \\ &= \text{Shaper} \\ &= \text{Circ}_{1\rightarrow 2} + \text{PC} + 2(\text{Col}) + \text{Circ}_{2\rightarrow 3} \\ &= 256.5\text{cm} + 386.7\text{cm} + 2(235.5\text{cm}) + 266.3\text{cm} \\ &= 1380.5\text{cm}. \end{aligned} \tag{A.2}$$

Next, the total fiber in the system was found. The fiber lengths in the entire system are listed in table A.3. A basic layout of the fiber lengths is given in figure A.2.

The final step was to calculate the total DCF and SMF required for dispersion compensation. The following set of equations were used with the appropriate numbers from table A.3.

$$\begin{aligned} T &= \text{Total Pulse Shaper Length} \\ &= DCF_{SIG} + DCF_{LASER} + SMF_{\tau} + DCF_{\tau} \\ &= DCF_{SIG} + DCF_{LASER} + (1+\alpha)DCF_{\tau}, \end{aligned} \tag{A.3}$$

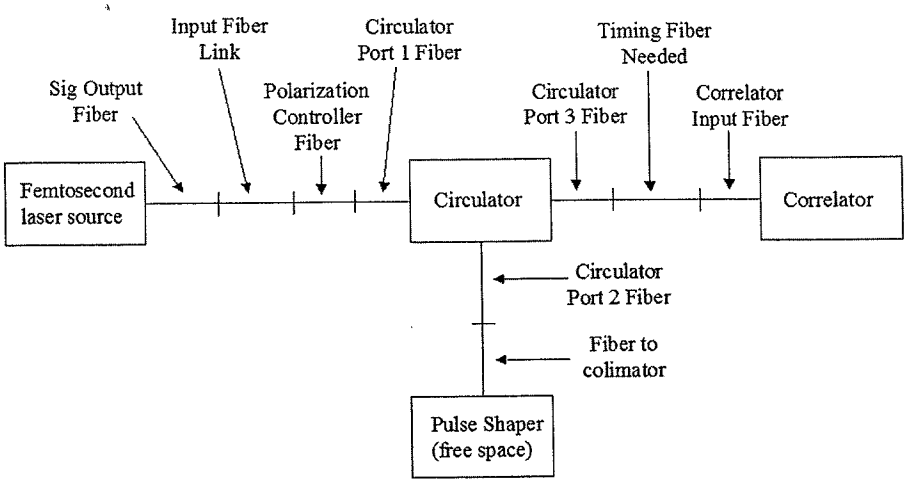

Fig. A.2. Fiber layout in entire system. Used to calculate DCF needed to compensate all SMF.

Table A.3

SMF lengths of all components in overall system that must be compensated for chromatic dispersion by DCF. The symbols located in this table are used for the calculations within this appendix. The term 'Experimental Fiber' refers to fiber originally intended for experimental research. The term 'Commercial Fiber' refers to fiber obtained from a commercial vendor in Denmark.

Mathematical Symbol	**System Component**	**Experimental Fiber**	**Commercial Fiber**
$Laser_{SIG}$	Laser output	63.6 cm	63.6 cm
$Shaper_{IN}$	Laser output to PC input	503.1 cm	503.1 cm
PS	Pulse shaper	1380.5 cm	1380.5 cm
T	Link to obtain timing	1856.8 cm	1856.8 cm
$Auto/XC_{IN}$	Auto-/Cross-corr. input	176.8 cm	176.8 cm
DCF_{LASER}	Internal laser residual	73.8 cm	42.1 cm

where α is the length (in meters) of SMF that can be compensated with 1 m of DCF.

$$\begin{aligned} DCF_{SIG} &= \text{DCF needed to compensate the signal path} \\ &= \frac{Laser_{SIG}+Shaper_{IN}+PS+AutoXC_{IN}}{\alpha}, \\ \\ DCF_{\tau} &= \text{DCF needed to compensate the timing fiber} \\ &= \frac{T-DCF_{SIG}-DCF_{LASER}}{(1+\alpha)}, \\ \\ SMF_{\tau} &= \text{SMF needed to compensate the timing} \\ &= T - DCF_{SIG} - DCF_{LASER} - DCF_{\tau}. \end{aligned} \tag{A.4}$$

Finally, the values of SMF_{link} and DCF_{link}, the amount of SMF and DCF, respectively, that needed to be put into the output link from the shaper to the cross-correlator input were found.

$$\begin{aligned} SMF_{link} &= SMF_{\tau}, \\ DCF_{link} &= DCF_{\tau} + DCF_{LASER} + DCF_{SIG}. \end{aligned} \tag{A.5}$$

where the SMF_{link}, SMF_{τ}, DCF_{link}, DCF_{τ}, DCF_{LASER}, and DCF_{SIG} are as given in table A.3.

A.3 Experimental Dispersion Compensating Fiber

Initially, a spool of DCF was used to build the dispersion compensating link. Based on equation A.5, in which values of $\alpha = 4.68$ and $DCF_{LASER} = 73.8$ cm were used, the link needed to consist of 1095.14 cm SMF and 761.55 cm DCF. When the link was built, however, the output pulse had problems with the dispersion. This was evident because the output pulse, with no shaping, had little in common with the pulse input to the system by the laser. In figure A.3, the laser input and the system output are shown for comparison.

After rebuilding the link two additional times and obtaining similar results, the characteristics of the experimental dispersion compensating fiber were investigated through the cutback method.

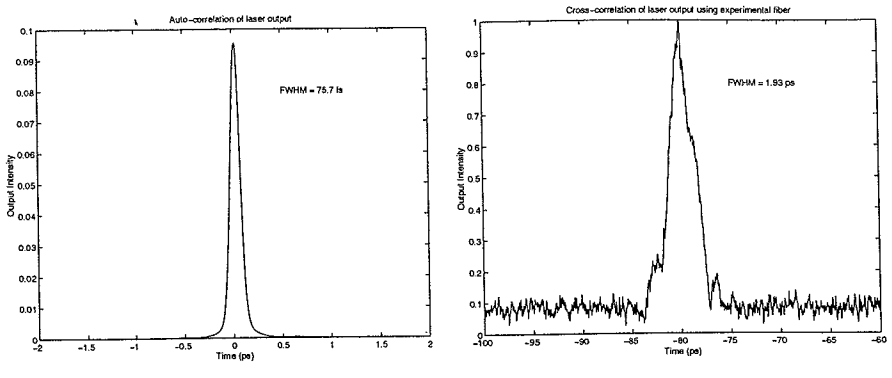

(a) Intensity auto-correlation of Reference signal (Laser Output), FWHM = 75.7 fs

(b) Intensity correlation of Output signal, FWHM = 1.93 ps

Fig. A.3. Intensity correlations using experimental DCF fiber.

A.3.1 Cutback Method

The cutback method consists of starting with a known length of SMF and DCF in a system and cutting back small amounts of DCF until an obvious minimum pulse width is obtained. The process is then repeated with the SMF until another minimum is obtained. While this process would cause an error in the timing of the system, it is possible because the measurements are taken using a time-independent auto-correlation measurement of the signal.

Best-fit curves of the Pulse FWHM vs. Fiber length were made for two sets of curves. One set of curves was developed through the use of fiber on the order of three times the length of fiber in the other set of curves. Two such sets of curves are shown in figure A.4. The curves labeled 'Ref link' are from the shorter set of fiber lengths and the curves labeled 'Sig link' are from the longer set of fibers.

The minimum pulse FWHM of each of the four figures were found using a second order best-fit line. A system of equations was then used to solve for α and DCF_{LASER} using equation A.6 and the minimums from the best fit lines as listed in table A.4.

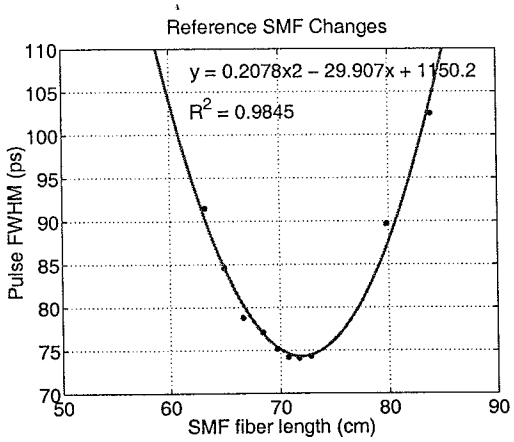

(a) Best fit curve of Reference Link SMF.

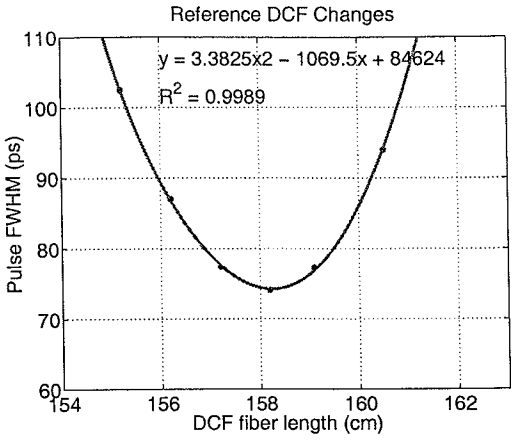

(b) Best fit curve of Reference Link DCF.

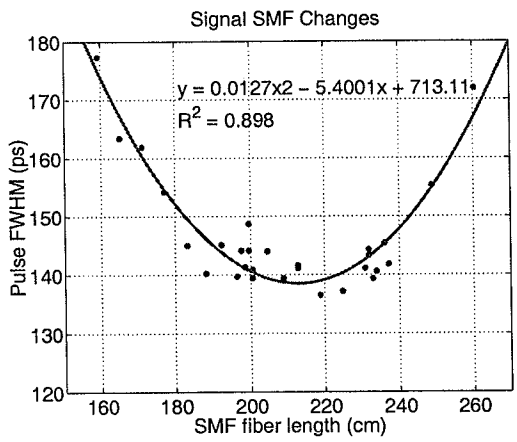

(c) Best fit curve of Signal Link SMF.

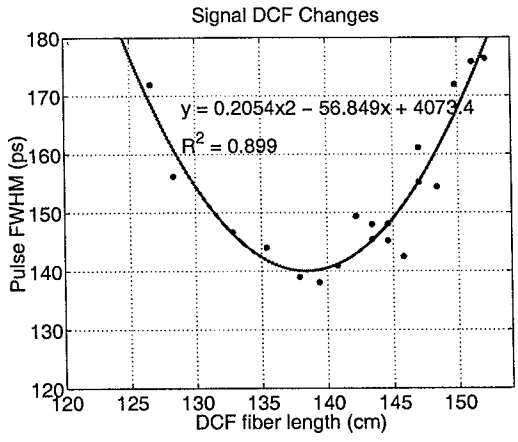

(d) Best fit curve of Signal Link DCF.

Fig. A.4. Example Dispersion Ratio Experiment Best Fit Curves.

$$\begin{aligned} DCF_{Reference} - \frac{SMF_{Reference}}{\alpha} &= DCF_{LASER}, \\ DCF_{Signal} - \frac{SMF_{Signal}}{\alpha} &= DCF_{LASER}. \end{aligned} \tag{A.6}$$

Solving equations A.6 yielded $\alpha = 4.1397$ and $DCF_{LASER} = 71.18$ cm, where DCF_{LASER} and α are as given in table A.3. These values were very different from those previously used to calculate the DCF needed in the system and were used to

Table A.4

Fiber lengths that obtained the minimum pulse widths during cutback methods. These numbers include all fiber in the entire system, not just the link being tested.

Fiber Test Name	Fiber Length
Reference Path SMF	359.76 cm
Reference Path DCF	900.04 cm
Signal Path SMF	3134.25 cm
Signal Path DCF	158.09 cm

produce another link. The new link once again resulted in similar results to those shown in figure A.3. The cutback method was performed a third time and resulted in values of $\alpha = 4.1272$ and $DCF_{LASER} = 299.81$ cm. With portions of DCF taken from the spool immediately after one another, the values of α and DCF_{LASER} were inconsistent with one another. A conclusion was made that the fiber characteristics were changing and different DCF needed to be obtained for the experimental setup.

A.3.2 Possible Causes for Changing Fiber Characteristics

When DCF fiber is made, glass with one refractive index is placed around a cylinder of glass with another refractive index. The composite glass is then 'stretched' until the desired fiber diameters are obtained. Thus, two possible explanations as to why the dispersion compensation characteristics of the experimental DCF fiber could have been changing are evident. The fiber on the spool could have been taken from the end of the several hundred kilometers of fiber that were developed at one time and the 'stretching' was not quite perfect. The equipment used could also have experienced a problem while the fiber was being made, causing the glass to have

different characteristics at the location from which the spool of 5 km used for the setup was taken from the overall fiber length.

A.4 Purchased Dispersion Compensating Fiber

Commercial DCF fiber was ordered. While the cost of a spool of 5 km of bare fiber was much more expensive than the experimental fiber, the results were very consistent and worth the expense. The cutback method was again performed to calculate the amount of SMF that could be compensated by 1 m of DCF. The final link for the pulse shaper apparatus was then made using the calculations and methods described in section A.2. The results are summarized here.

A.4.1 Cutback Method and Results

The cutback method was first performed on the commercial DCF. $DCF_{LASER} =$ 42.1 cm and $\alpha = 7.4719$ were calculated from the results using the same set of equations as in section A.3.1. A new dispersion compensating link was then built using the fiber and inserted into the system. The link consisted of 507.05 cm DCF and 1349.80 cm SMF.

There are two signals shown in figure A.5. One signal is the auto-correlation of the reference pulse directly from the laser. The other signal shows the result from an intensity cross-correlation when the pulse shaper is included, but with no spectral phase compensation implied by an LCM.

It is clear from figure A.5 that the dispersion compensation of the commercial fiber was more effective than the experimental fiber. However, as depicted by table A.1, a cubic dispersion was present.

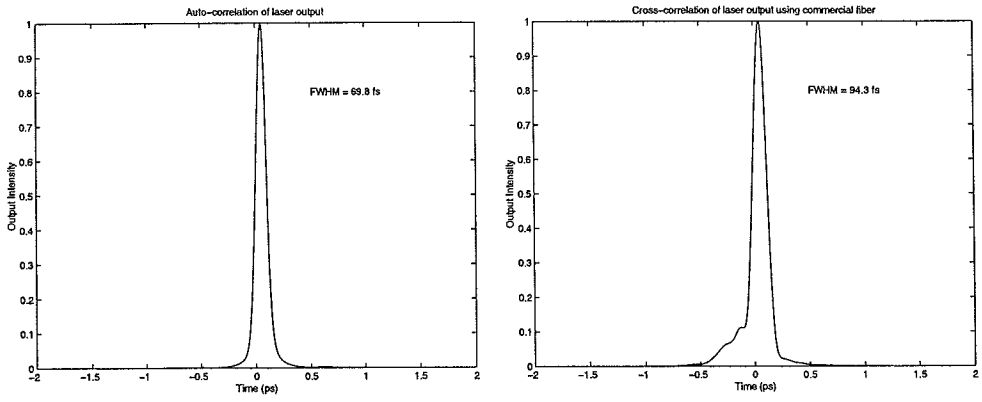

(a) Laser output intensity autocorrelation, deconvolved FWHM = 69.8 fs

(b) Signal intensity correlation, deconvolved FWHM = 94.3 fs resulting with sig link XC

Fig. A.5. Reference and Signal correlations using commercial fiber.

APPENDIX B
LCM CALIBRATION

The LCMs must be calibrated prior to use. The LCM in practice is calibrated and used in conjunction with a single set of electronics to minimize the possibility of error when the voltage 'levels' are applied on the LCM in order to achieve the desired phase on the spectrum.

Figure B.1 shows the calibration system for an LCM, placed in conjunction with the reflective pulse shaper apparatus. In addition to the calibration configuration shown, the calibration components can be placed between the collimator and grating or the grating and the lens, using the most convenient arrangement. The polarizer negates polarization fluctuation. The beam splitter is used to separate the reference path and the signal path. The detection of a reference signal is used to monitor power fluctuation during the calibration process. Finally, the signal beam is sent to the signal detector after it is reflected from the mirror. Assuming an induced phase shift of Φ_A and Φ_B from the two layers of the liquid crystal, the light experiences a transmission T and phase shift Φ as follows [15]:

$$T = cos^2\left(\frac{\Phi_A - \Phi_B}{2}\right), \tag{B.1}$$

where

$$\Phi = \frac{\Phi_A + \Phi_B}{2}. \tag{B.2}$$

In the two-layer LCM, the layers need to be calibrated individually by setting one layer to the maximum level, 4096, and then scanning the other layer across all possibile voltage 'level' values $(0 - 4096)$. As an example of the resultant calibration curve raw data, the single-layer LCM calibration obtained when the calibration procedure was performed is shown in figure B.2. The transmission intensity curve shows

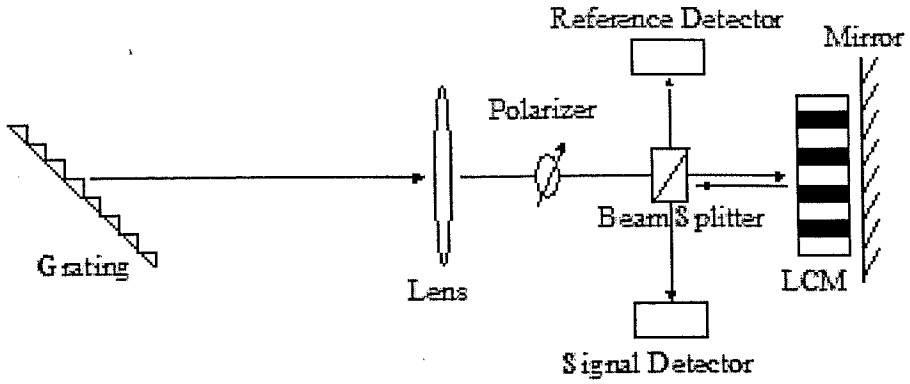

Fig. B.1. The LCM calibration is performed in a pulse shaper. A polarizing beam splitter separates the reference and signal paths, both of which are measured by power detectors.

$T_A - V_A$ where T_A is the transmission voltage detected and V_A is the voltage applied to the layer being cailbrated.

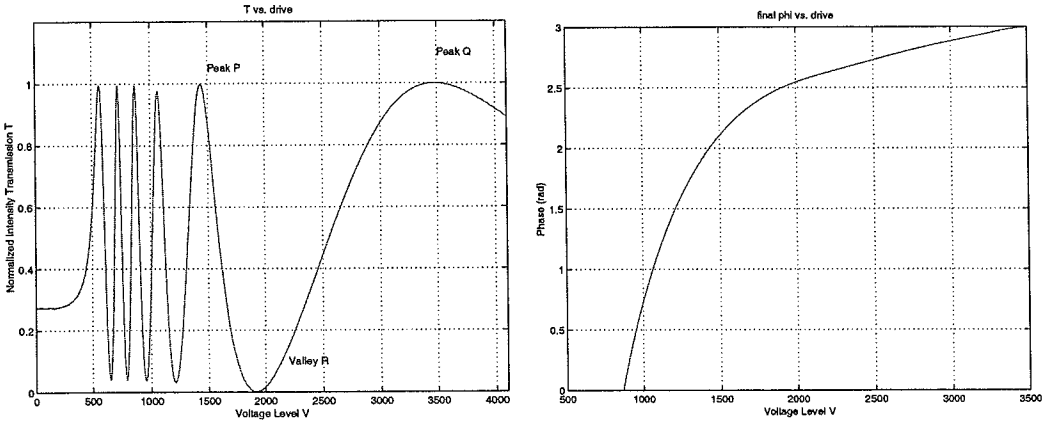

(a) Raw Data Transmission Curve.

(b) Extracted data calibration curve.

Fig. B.2. Sample transmission raw data curve and extracted calibration curve from LCM calibration procedure.

Data processing can be used to extract the phase-voltage relationships of the curve [25]. For the single-layer LCM system, the QWP creates a single-pass pulse

shaper, as described in 4.3. Thus, a 2π phase range for control is obtained through the following procedure because the calibration process is performed in a double-pass system.

1. Select any two ajacent minimums or maximums to extract 2π phase-voltage data (refer to equations B.1 and B.2). In order to optimize the results, the two peaks furthest away from one another, P and Q on figure B.2, are chosen.
2. Obtain the phase shift for the first layer by first getting the phase shift from P to R by using the relationship $\Phi_A = 2cos^{-1}(\sqrt{T_A(V_A)})$.
3. Obtain the phase shift for the remainder of the first layer by using the relationship $\Phi_A = \left[2\pi - 2cos^{-1}(\sqrt{T_A(V_A)})\right]$ where Φ_{B4095} is the same value as in the previous step.
4. Perform curve fitting to smooth the resultant $\Phi_A - V_A$ curve.
5. Repeat steps $1-4$ for another 2π range immediately adjacent to the previous selection. Add 2π to the range obtained.
6. Through this method, the phases that have been obtained are the total phase values that are applied on the signal. Thus, the calibration curve can be used directly.